https://doi.org/10.1142/9789811278952_0005

Chapter 5

Machine Physics and Performance

G. Arduini, R. De Maria, M. Giovannozzi, G. Iadarola, E. Métral,
Y. Papaphilippou and R. Tomás

CERN, BE Department, Genève 23, CH-1211, Switzerland

The main beam and machine parameter choices and the underlying beam dynamics considerations are reviewed together with the main challenges and expected performance.

1. Overview of the Performance Goals and Main Choices

The maximum instantaneous luminosity L_{inst} of the HL–LHC will be limited by the maximum event pile-up per bunch crossing that the high luminosity experiments ATLAS and CMS, located at the Interaction Points (IP) 1 and 5 respectively, will be able to handle. After the upgrade they are expected to cope with values of at least 140 and up to 200 events per bunch crossing. These values correspond to instantaneous luminosities of approximately 5×10^{34} cm^{-2}s^{-1} and 7.5×10^{34} cm^{-2}s^{-1} for the maximum number of bunches that can be injected in the LHC (approximately 2750).[1] The HL–LHC project[2,3] aims to achieve a 'virtual' peak luminosity that is considerably higher than the maximum imposed by the acceptable event pile-up rate, and to control the instantaneous luminosity to a lower value L_{lev} during the physics fill ('luminosity levelling') so that the luminosity production can be sustained over longer periods to maximize the integrated luminosity. The luminosity evolution can be estimated taking into account the beam population N_{beam} reduction due to the collisions (the so called 'burn-off') in n_{IP} collision

points[4] as

$$\frac{dN_{beam}}{dt} = -n_{IP}\sigma_{tot}L_{inst} \ , \tag{1}$$

where the burn-off cross-section has been conservatively taken to be the total cross-section σ_{tot} (111 mb at 7 TeV[1,5]). No other sources of intensity reduction or emittance blow-up are considered in this simplified model. In operation with luminosity levelling an effective beam lifetime τ_{eff} can be defined from Eq. (1) as,[4,6]

$$\tau_{eff} = \frac{N_{beam}}{n_{IP}\sigma_{tot}L_{lev}} \ , \tag{2}$$

illustrating that τ_{eff} is proportional to beam intensity. Figure 1 shows the expected yearly-integrated luminosity as a function of the 'virtual' peak luminosity L_{virt} for $L_{lev} = 5 \times 10^{34}$ cm^{-2}s^{-1} and 7.5×10^{34} cm^{-2}s^{-1}. The corresponding optimum fill length (i.e. the length of time for each fill that will maximize the average luminosity production rate) is also shown. The annual integrated luminosity is determined for a minimum turnaround time of 145 minutes,[7] a scheduled physics time for luminosity production of 160 days per year with an efficiency for physics (defined in Ref. [8,9]) of 50%. In order to reach the goal of integrating 250 fb^{-1}/year the peak virtual luminosity L_{virt} must exceed 1.5×10^{35} cm^{-2}s^{-1} if $L_{lev} = 5 \times 10^{34}$ cm^{-2}s^{-1}. Larger values are of particular interest if $L_{lev} = 7.5 \times 10^{34}$ cm^{-2}s^{-1} or higher.

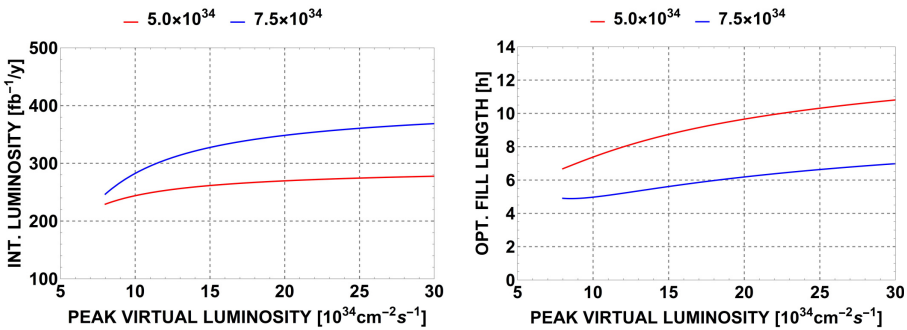

Fig. 1. Left: Expected annual integrated luminosity. Right: optimum fill length as a function of the 'virtual' peak luminosity L_{virt} for $L_{lev} = 5 \times 10^{34}$ cm^{-2}s^{-1} and 7.5×10^{34} cm^{-2}s^{-1}. A circulating current of 1.1 A (corresponding to $N_{beam} = 6.1 \times 10^{14}$p) and two ($n_{IP}$=2) high-luminosity IPs have been assumed.

The instantaneous luminosity L_{inst} is given by:[10]

$$L_{inst} = \frac{n_b N^2 f_{rev} \gamma}{4\pi\beta^* \epsilon_n} R(\beta^*, \sigma_z, d_{bb}) \tag{3}$$

where n_b is the number of colliding bunches per beam, N is the bunch population, f_{rev} is the beam revolution frequency, γ is the relativistic gamma factor and assuming equal R.M.S. normalized emittances ϵ_n in collision for both beams and transverse planes. The Twiss beta function β^* at the IP determines, together with ϵ_n, the R.M.S. beam size $\sigma^* = \sqrt{\epsilon_n \beta^* / \gamma}$ at the IP (assuming that the contribution to the beam size due to the dispersion and the momentum spread of the beam can be neglected). Here and below it is assumed that the beam is ultra-relativistic.

A crossing angle θ_c is needed to separate bunches immediately upstream and downstream of the IP to avoid unwanted parasitic collisions. This leads to a reduced geometric overlap between the colliding beams, and hence to a reduction in luminosity. The crossing angle needs to be increased when reducing the β^* in order to maintain a sufficiently large normalized long−range beam−beam separation d_{bb}, defined as $d_{bb} = \theta_c \beta^* / \sigma^*$. The luminosity is also reduced by the "hourglass effect" that arises from the increase of the β function upstream and downstream of the IP along the bunch longitudinal distribution. The hourglass effect is enhanced by a reduction in β^* and by an increase in bunch length σ_z. The luminosity reduction factor R in Eq. (3) takes both the crossing angle and the hourglass effect into account. Equation (3) shows the parameters that can be varied to maximize the instantaneous luminosity. The following considerations have been used as guidelines to define the HL–LHC machine and beam parameters at the project conception:[11]

- The maximum number of bunches n_b is limited by:
  - the minimum time interval between bunch crossings at the IP that can be handled by the detectors: this is limited to 25 ns;
  - the maximum number of bunches n_{SPS} that can be transferred safely from the SPS to the LHC;
  - the rise-time of the injection kickers in the SPS and LHC, extraction kickers in the PS and SPS, and abort gap kicker in the LHC;
  - the need to inject one train consisting of a few bunches (typically 12 nominal bunches for 25 ns spacing), for machine protection

considerations, before injecting one nominal batch;[12]
  - the need for non-colliding bunches for background evaluation by the experiments and a sufficient number of collisions for the lower luminosity experiments.[13]

- The maximum bunch population N should be well below the single bunch Transverse Mode Coupling Instability (TMCI) threshold in the LHC, expected to be 3.5×10^{11} p/bunch.[14]
- The maximum cryogenic power available to cool the beam screen limiting the beam current circulating in the LHC, $I_{beam} = eN_{tot}f_{rev}$ (where e is the proton charge and N_{tot} the total beam population) to approximately 1.1 A.[15]
- The total available power for the main 200 MHz SPS RF system after the LHC Injector Upgrade limiting the maximum bunch population to $N_{SPS} = 2.4 \times 10^{11}$ protons at SPS extraction for 288 bunches. An intensity loss of about 5% distributed along the cycle is assumed from SPS extraction to collisions in the LHC.
- The beam brightness $B = N/\epsilon_n$ is limited by:
  - The maximum brightness achievable in the injectors $B_{SPS} \approx 1.5 \times 10^{11}$ p/μm after the full injector upgrade[16]
  - The total head–on beam–beam tune shift $\Delta Q_{bbHO} \approx 0.03$.[11]
  - Intra–beam scattering (IBS) inducing transverse and longitudinal emittance blow–up, particularly at injection but also in the acceleration, squeeze, and collision phases.
- The minimum β^* is constrained by:[17]
  - The triplet aperture as the beam size at the triplet and $\theta_c = d_{bb}\sqrt{\epsilon_n/\gamma\beta^*}$ required to maintain a sufficiently large normalized beam—beam long–range (BBLR) separation d_{bb} and minimize the corresponding tune spread ΔQ_{bbLR} increase with $1/\sqrt{\beta^*}$;
  - The maximum β function at the triplet that can be matched to the regular optics of the arcs within the distance available in the matching section between the triplets and the arcs;
  - The strengths of the arc sextupoles available to correct the chromaticity generated by the triplets (proportional to the maximum value of the β function β_{max}).

Table 1 shows the beam parameters in collision, selected on the basis of the above considerations.

Table 1. HL–LHC nominal parameters for 25 ns operation[18,19] for two production modes of the LHC beam in the injectors.[8]

Parameter	Nominal LHC (design report)	HL–LHC (standard)	HL–LHC (BCMS)[#]
Beam energy in collision [TeV]	7	7	7
Particles per bunch, N [10^{11}]	1.15	2.2	2.2
Number of bunches per beam	2808	2760	2744
Number of colliding bunches in IP1 and IP5[*]	2808	2748	2736
Total beam population N_{tot} [10^{14}]	3.2	6.1	6.0
Beam current [A]	0.58	1.10	1.10
Half-crossing angle in IP1 and IP5 [μrad]	142.5	250	250
Minimum norm. beam—beam long–range separation [σ]	9.4	10.5	10.5
Minimum β^* [m]	0.55	0.15	0.15
ϵ_n [μm]	3.75	2.50	2.50
Longitudinal emittance ϵ_L [eVs]	2.50	3.03	3.03
R.M.S. energy spread [10^{-4}] (q-Gaussian distribution)	-	1.1	1.1
R.M.S. energy spread [10^{-4}] (FWHM equiv. Gaussian)	1.13	1.29	1.29
R.M.S. bunch length [cm] (q–Gaussian distribution)	-	7.61	7.61
R.M.S. bunch length [cm] (FWHM equivalent Gaussian)	7.55	9.0	9.0
IBS horizontal [h]	105	16.5	16.5
IBS longitudinal [h]	63	19.2	19.2
Radiation damping [h]	26	26	26
Piwinski parameter	0.65	2.66	2.66
Total reduction factor R_0 without crab cavities at min. β^*	0.836	0.342	0.342
Total reduction factor R_1 with crab cavities at min. β^*	-	0.716	0.716
Beam–beam tune shift/IP [10^{-3}]	3.1	8.6	8.6

Table 1. (*Continued*)

Parameter	Nominal LHC (design report)	HL–LHC (standard)	HL–LHC (BCMS)[#]
Peak luminosity without crab cavities L_{peak} [10^{34} cm^{-2}s^{-1}]	1.00	8.11	8.07
Peak luminosity w. crab cavities $L_{virt} = L_{peak}R_1/R_0$ [10^{34} cm^{-2}s^{-1}]	-	17.0	16.9
Events/crossing w/o levelling and without crab cavities	27	212	212
Levelled luminosity [10^{34} cm^{-2}s^{-1}]	-	5.0	5.0
Events/crossing μ (with levelling and crab cavities)	27	131	132
Max. line density of pile–up events during fill [evts/mm]	0.21	1.3	1.3
Levelling time [h] (assuming no emittance growth)[‡]	-	7.4	7.3
Number of collisions in IP2/IP8	2808	2492/2574[**]	2246/2370[**]
N at injection [10^{11}][††]	1.20	2.30	2.30
Maximum number of bunches per injection N_{SPS}	288	288	240
Total beam population per injection [10^{13}]	3.46	6.62	6.62
ϵ_n at SPS extraction [μm][‡‡]	3.50	2.10	1.70

[#] BCMS parameters are only considered for injection and as a backup parameter set in case one encounters larger–than–expected emittance growth in HL–LHC during injection, ramp, and squeeze.

[*] Assuming one less batch from the PS for machine protection (pilot injection, transfer line steering with 12 nominal bunches) and non-colliding bunches for experiments (background studies, etc.). Note that due to RF beam loading the abort gap length must not exceed the 3 μs design value.

[‡] The total number of events/crossing is calculated with an inelastic cross–section of 81 mb, while 111 mb is assumed as a pessimistic value for calculating the proton burn off and the resulting levelling time.[1,5]

[**] The lower number of collisions in IR2/8 compared to the general-purpose detectors is a result of the agreed filling scheme, aiming as much as possible at an equal sharing of collisions between the experiments.

[††] An intensity loss of 5% distributed along the cycle is assumed from SPS extraction to collisions in the LHC.

[‡‡] A transverse emittance blow–up of 10-15% on the average H/V emittance in addition to that expected from IBS is assumed (to reach 2.5 μm of emittance in collision for 25 ns operation).

In addition the following main choices have been made to enhance L_{virt}:[20]

- installation of large aperture triplet quadrupoles close to the IP to allow sufficient aperture for large crossing angles and small β^*;
- installation of crab cavities, i.e. RF deflecting cavities providing opposite transverse kicks to the head and tail of the bunches upstream and downstream of the IP to suppress the crossing angle at the IP and provide head-on collisions.

2. Optics and Layout Choices

As mentioned above, the smaller values of β-function at the interaction points impose the use of large-aperture magnets. In addition, the higher luminosity implies also a larger amount of collision debris that should be absorbed outside the coils of the superconducting magnets to avoid depositing energy there, thus inducing the risk of quenching or reducing the magnets' lifetime. This means that the larger coil aperture shall be used not only for increasing the available space for the beams, but also for installing appropriate shielding materials. Furthermore, external absorber devices have to be added to the layout to provide additional shielding power. These devices are either fixed masks, installed in front of the superconducting magnets, or collimators with movable jaws. It is worth stressing that the larger coil aperture of the triplet quadrupoles imposes the use of a new technology for the superconducting cable, Nb_3Sn based cables instead of Nb-Ti as in the LHC. The length and strength of the triplets has been optimized to reduce the peak-β function in the triplets,[21] compatibly with the hardware constraints, in order to reduce the smallest reachable β^* and the optical aberrations.

Two more aspects have been considered in the design of the new layout, namely the optimisation of the crab cavities and the system of orbit correctors used to generate the separation and crossing angle bumps. Crab cavities require well-defined optical conditions (large β functions) to be fulfilled in order to achieve optimal performance. The system of orbit correctors has been also highly optimised[22] to reduce the strength needs without compromising its performance or that of the crab cavities.[23] A final improvement has been provided by the implementation of a full remote alignment system[24] that allows a substantial reduction of the required strength. The latest layout of the new

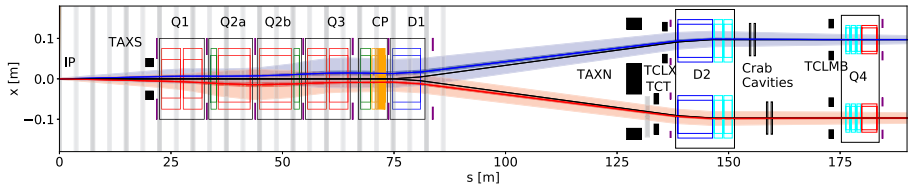

Fig. 2. Overall layout of the insertion region between the IP and Q4. The dark blue and dark red areas represent the 2σ beam envelope for the $\beta^* = 15$ cm round optics. The lighter regions correspond to the 11.9σ value of the beam envelope for a normalized emittance of 2.5 μm and including tolerances in β-beating and orbit distortions. This represents the required minimum beam-stay clear in the IR magnets shown to be protected by the collimation system in collision. The shaded grey areas in the triplet region represent the locations of the parasitic beam-beam encounters in which the BPM (marked in purple) should not be installed.

insertions, i.e. version 1.4, is shown in Figure 2 for the region between the interaction point and the Q4 quadrupole, including TAXS, TAXN (collision debris absorbers), D1, D2 (combination separation dipoles), and TCLX-TCTX (tertiary collimators).

Note that the HL–LHC layout has been incrementally updated since version 1.0[25–27] following the development of the new hardware, cost optimisation exercises, new requests from the experiments, and also the experience gathered during the LHC Run 2[28–30] (the comprehensive and up-to-date list of the changes with respect to the LHC layout is available in Ref. [20]).

As far as the optics is concerned, different settings of the experimental insertions[31] elements provide the conditions for the proton[7] and ion programmes,[32] as well as special runs for luminosity calibration (the so-called Van der Meer scans). The baseline scenario of the proton programme relies on the Achromatic Telescopic Squeeze (ATS) optics scheme[33] with equal $\beta^* = 15$ cm in the transverse planes (so-called round optics). Alternative configurations, based on optical solutions featuring unequal β^* values in the transverse planes are also available (so-called flat optics). The advantage of flat optics is that a smaller-than-nominal β^* value can be used in the plane orthogonal to the crossing plane (as low as 7.5 cm), while a larger one is used in the crossing plane (see Section 8). Note that for the proton physics runs, the ALICE experiment is supposed to take data with $\beta^* = 10$ m, while LHCb with β^* as low as 1.5 m to provide the necessary luminosity for the possible LHCb Phase-II upgrade.[34] For the ion programme, low β^* optics have been

designed for all experiments (50 cm for ATLAS, ALICE, CMS, and 1.5 m for LHCb).

Luminosity levelling is assumed in all experiments, which is achieved by varying β^* and the crossing angle (for ATLAS and CMS), or the parallel separation (for ALICE and LHCb). This implies that a dynamic change of the optics is part of the collision process. Nevertheless, one should consider that the injection and collision optics are different. An optics transition is performed during the energy ramp[35] so that at the end of the energy ramp, the optics is ready for bringing the beams into collisions.

As a last point, the overall HL–LHC ring optics has been reviewed and improved also in the non-experimental insertions. Worth mentioning is the optics in IR4, hosting the RF cavities and most of the instrumentation devices, which fulfills the specific constraints for RF cavities, pick-ups, kickers, and beam profile measurement devices, as well as suitable optical conditions for the possible use of electron lenses.[36] Furthermore, the optics in IR6, hosting the beam dump, has been developed so to fulfill special phase advance constraints needed for machine protection considerations.[37,38]

3. Linear Optics Correction and Specification for Power Converter Performance

Optics control in the HL–LHC is challenging due to the very low β^* of 15 cm at the two high luminosity IPs and the increased β functions in the arcs during the telescopic squeeze. The peak β–beating achieved in LHC in the range between 7% and 11%[39–41] cannot be guaranteed for HL–LHC. Simulations[42] and experiments[43] suggest that a peak β–beating of 20% is a more realistic target, which was then used to define the aperture margins of the machine.[44] The tightest tolerance on optics comes from the experiments requiring a luminosity imbalance not larger than 5%, which requires a β^* control to better than 2.5% at the IPs. To measure β^* the gradient of the quadrupoles closest to the IP are modulated while measuring the tune. This technique is called K–modulation.[45,46] In the following all HL–LHC hardware aspects relating to optics control and new possible measurement techniques are discussed.

The tight tolerances in the optics control impose tight requirements on the magnetic measurement and powering precision as well as on alignment. For illustration, a Gaussian error distribution in the integrated gradient of

the HL–LHC triplet quadrupoles with a R.M.S. of 10^{-4} produces a R.M.S. β–beating of 7.2% at β^*=15 cm.

The integrated gradient of HL–LHC triplet quadrupoles will be within 0.1% standard deviation of the design value, which is the accuracy of the measurement. The precision of the measurement is $\pm 2 \times 10^{-4}$ which allows pairing quadrupoles of similar strength within the Q2 module.[48]

The longitudinal location of the nodal points of the triplet quadrupoles are expected to follow a uniform distribution with a maximum deviation of ±2 mm. For a definition of nodal points see.[49] Similarly, the magnetic length has an accuracy of ±5 mm.[49] The tilt angle around the beam axis of each quadrupole in the triplet is specified to be within ±2 mrad, while the measurement accuracy of the average tilt of the two quadrupoles in a cold mass is ±0.5 mrad. The local magnetic field angle in each section of the quadrupole should be within ±2 mrad[49] from the average field angle of the whole magnet.

The accuracy of β^* from K–modulation is determined by the knowledge of the integrated gradient and alignment of the closest quadrupoles to the IP (Q1A left and right to the IP) and of the machine tune drifts over the time scale of the measurement. The resolution of the tune measurement contributes to the β^* uncertainty and therefore needs to be optimized by correcting chromaticity and amplitude detuning and further reduced thanks to repeated measurements.

Table 2. Power converter stability specifications for HL–LHC circuits. All uncertainties are 2σ in units of $10^{-6} I_{rated}$, where σ is the rms.[50]

Circuit name	I_{rated} [A]	PC class	Stability 20 min	12 h
RB[a], RQ(D/F)[a]	13000	1	0.4	2
RQX	18000	0	0.2	1
RTQX(1/3), RCBX	2000	2	1.2	15.5
RTQXA1[b]	60	4	5	40
RQSX[d], RCBRD, RTB9[c]	600	3	2	34
RC(S/O/D/T)X, RCB(C/Y)[a]	120	4	5	40
RD(1/2)	14000	0	0.2	1
RQ4[a]	4000	2	1.2	15.5
RQ(5/6)[a]	5000	2	1.2	15.5

[a] Existing circuit assumed not to be upgraded.

[b] Compatible with the use of the trim as I_{max} = 35 A in operation.

[c] Standard 600 A PC is assumed even though I_{max} = 250 A in operation.

[d] Standard 600 A PC is assumed even though I_{max} = 200 A in operation.

From power converter (PC) stability specifications, Table 2,[50] tune drifts can be estimated and used in realistic simulations of K–modulation incorporating all mentioned uncertainties.[51]

As a benchmark the tune jitter was measured in LHC for various optics and compared to expected values from power converter specifications.[52] Model predictions were close or below measurements by up to a factor 2. This might indicate that there are other sources of tune drifts not yet identified, making current simulations optimistic. Figure 3 (left) shows the expected β^* accuracy from K–modulation versus β^* and assuming that the tune jitter, δQ, scales as $1/\beta^*$, which is confirmed in simulations. The tune modulation amplitude is also scaled with $1/\beta^*$ as the Q1A maximum current is 35 A. The maximum tune modulation is limited to 0.01 to avoid beam loss. The green curve corresponds to the current HL–LHC baseline having a β^* accuracy of 7.5% at β^*=15 cm and reducing to the target of 2.5% at β^*=25 cm. The yellow curve corresponds to an upgrade of the ATS arcs' dipole power converters to class 0 (see Chapter 11 for the definition of the classes of power converters). The β^* accuracy is improved to 4% at β^*=15 cm. The point at β^*=7.5 cm corresponds to the case of a flat optics with $\beta^* = 30/7.5$ cm and the β^* uncertainty is as large as 33% without any upgrade of the main dipole PC stability. The upgrade here also improves accuracy by a factor 2 but still remaining far from the target. Figure 3 (right) shows the contributions to the β^* uncertainty when

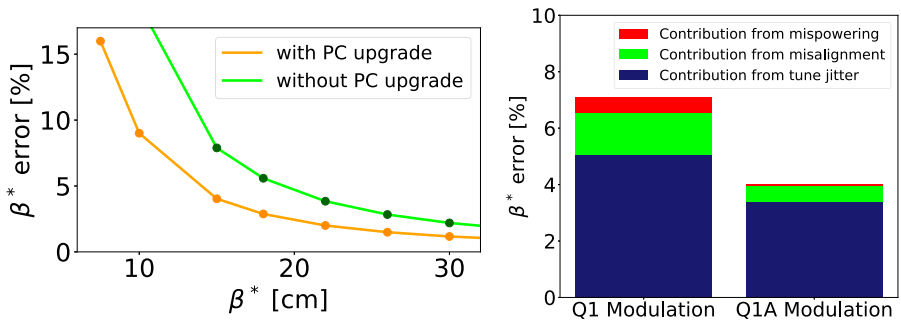

Fig. 3. Left: Expected β^* accuracy from K–modulation versus β^* for the current HL–LHC baseline (green) and an upgrade of the ATS arcs' dipole power converters to class 0 (yellow). The case with β^*=7.5 cm corresponds to the flat optics with $\beta* = 30/7.5$ cm. Right: contributions to the β^* accuracy when modulating Q1A and the two modules of Q1 at β^*=15 cm and $\delta Q = 2.9 \times 10^{-5}$ (upgraded of four dipole power converters to class 0).

modulating only the Q1A current and when the current of both Q1 magnets is modulated at β^*=15 cm and $\delta Q = 2.9 \times 10^{-5}$, being the tune jitter the largest contribution in both cases. Modulating only Q1A improves β^* accuracy by almost a factor 2 at β^*=15 cm. For that reason an independent trim circuit has been added to allow modulating the strength of the Q1A magnet.[53,54] Since the Q1A tune modulation amplitude decreases with β^* the full Q1 should be used for K–modulation measurements above β^*=25 cm.

As mentioned above, these estimates are optimistic as unknown sources of tune jitter may appear, yet the HL–LHC baseline does not reach the target β^* measurement accuracy. Alternative or complementary β^* control techniques will be required in HL–LHC. Luminosity waist scans have been experimentally tested in Run 2, demonstrating a performance better than K–modulation in the measurement of the waist location, as shown in Figure 4.[55] Yet, these scans cannot measure the individual β^* in the different planes and beams. Therefore Beam Position Monitors (BPM) with better resolution, such as those equipped with the DOROS electronics,[56] will also be needed in HL–LHC to measure the β at the waist location from the phase advance across the interaction region drift.[55] Optics-measurement-based BPM calibration techniques[57] will be needed to further improve measurement results. Machine learning techniques are also being explored.[58,59]

The triplet quadrupole tilt errors are corrected by minimizing the coupling resonance driving terms from beam measurements. Assuming the above tilt

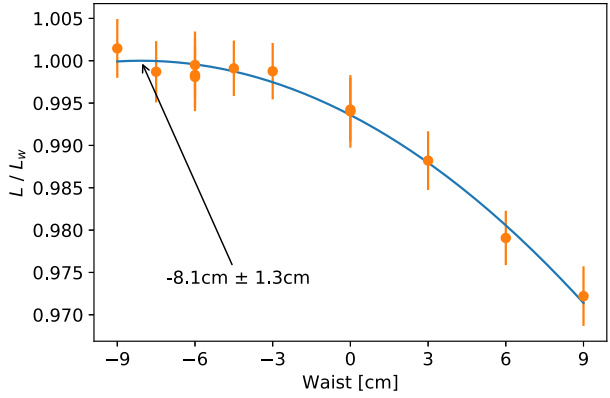

Fig. 4. Luminosity waist scan as proof-of-principle for accurate waist position measurement.[55]

tolerances there is about a factor 2 margin in the strength of the triplet skew quadrupole corrector, MQSX.[55] Imperfect local coupling correction at the IP can lead to luminosity loss even with perfect global coupling. HL–LHC luminosity is about a factor 4 more sensitive to left-right unbalanced MQSX coupling correction than LHC.[60,61] A technique to improve the locality of the coupling correction was tested in 2018 by applying a rigid shift of all IP betatron waists.[62]

The completion of the linear optics commissioning requires that non-linear corrections are in place to avoid beam losses while exciting forced betatron oscillations, to ensure high quality tune measurements and to minimize feed-down effects. Chapter 28 describes the various challenges involved in the non-linear commissioning.

The HL–LHC triplet Nb_3Sn superconductor features an unstable behaviour when subject to a change in voltage. This is referred to as "flux jumps". Measurements have revealed that these are expected to happen in the first half of the energy ramp, inducing a relative change in the gradient by about 0.2×10^{-4} with a rise time of about 50 ms. Simulations of flux jumps on orbit,[63] tune and emittance growth[64] show that these do not pose a threat for the HL–LHC performance.

4. Dynamic Aperture and Field Quality

Dynamic aperture (DA) is defined as the average amplitude in transverse phase space where the oscillation amplitudes remain within the defined mechanical aperture over a specified time interval. It is one of the key quantities for the design of modern colliders, based on superconducting magnets, such as Tevatron,[65–67] HERA,[68–71] RHIC,[72] and the CERN Large Hadron Collider (LHC) (see e.g., Ref. [47] for a detailed overview). Note that the DA reduces typically with increasing time intervals and that for design purposes it is customary to assume a conservative definition based on the minimum amplitude.

In a mathematical sense, stable motion implies bounded motion for arbitrary time, whereas in a physical context, particle stability can be linked to a maximum number of turns, $N_{\max}$, which depends on the specific application, for which bounded motion occurs. If an ensemble of initial conditions defined on a polar grid ($x = r\,\cos\theta\,,\;\; y = r\,\sin\theta\;\; 0 \leq \theta \leq \pi/2$, where x, y are expressed in units of σ_x, σ_y of the beam dimension) is tracked for up to $N_{\max}$

turns to assess their stability, then the DA can be defined as:[73]

$$DA(N) = \frac{2}{\pi} \int_0^{\pi/2} r_s(\theta; N)\, d\,\theta \equiv \langle r_s(\theta; N) \rangle_\theta \,. \tag{4}$$

where $r_s(\theta; N)$ stands for the last stable amplitude (disregarding any stable domain disconnected from the origin) for up to N turns in the direction θ, for $N < N_{\max}$. Given the choice of the co-ordinates, $DA(N)$ is expressed in units of beam sigma. The DA can be considered a function of time and whenever its border is inside the phase-space region occupied by the beam, particles will be pushed towards high amplitudes and eventually lost. This is the essence of the proposed relationship between DA and particles losses,[74] namely

$$\frac{I(N)}{I(1)} = 1 - \int_{DA(N)}^{+\infty} e^{-\frac{r^2}{2}}\, r\, dr = 1 - e^{-\frac{D^2(N)}{2}}, \tag{5}$$

where $I(N)$ represents the beam intensity at turn N. The relation (5) establishes a direct link between DA and losses and can be used to model the beam lifetime. In this way, the possibility to set a tolerances on the DA based on the target beam losses or lifetime is is available. This provides a very solid approach, based on physical observables such as losses, in the design phase of a particle accelerator. Parenthetically, Eq. (5) is the basis of an innovative method to experimentally determine the DA,[75] which complements the standard method,[76] as well as of novel models to describe luminosity evolution in the presence of burn off and losses due to DA.[77,78] DA computation consists of simulating the evolution of a large number of initial conditions, distributed to provide good coverage of the phase space under study. Given the CPU-intense nature of these simulations, studies explored techniques for finding easy-to-compute dynamical quantities, such as the so-called early indicators,[79] or to achieve parallelisation over the initial conditions.[80] In addition, models to fit, and eventually extrapolate, the dependence of the DA on the number of turns[81–83] have been looked for. The idea behind is that long-term behaviour of the DA, a computationally heavy task, can be extrapolated from numerical simulations performed over a smaller number of turns. Recently, refined models have been proposed[83] that improve the numerical stability of the model parameters: this paves the way to determine and study the dependence of the model parameters on the HL–LHC configuration in view of optimising the overall performance, also extrapolating to realistic time scales. In this respect, the approach studied seems mature, allowing the standard paradigm

of analysing the DA at a fixed number of turns to be abandoned, and instead considering the properties of its extrapolation and of the model parameters. It is worth stressing that these advanced techniques rely on a modern tracking code and postprocessing tools. The `SixTrack` code[84] is in fact kept up-to-date thanks to a vigorous plan aimed at improving and developing it.[85]

For the sake of completeness, it is important to mention that in parallel to the activities aimed at achieving a better understanding of the DA, research work is carried out to develop new diffusive models[86,87] to describe the beam dynamics in the HL–LHC, using the LHC as an experimental test bed. The novelty of this research is the functional form of the diffusion coefficient that is derived from the stability-time estimate of the Nekhoroshev theorem,[86,87] which has been proven to be compatible with experimental results. Following these encouraging outcomes, the next steps will be to establish a relationship between the approach based on the DA and that based on the diffusion equation, the use of symplectic tracking to compute the diffusion coefficient, and then to predict the beam distribution evolution, including also noise effects.

Part of these concepts have been applied to the analysis of the DA of the HL–LHC, whose main results have been collected in Ref. [88]. Detailed studies of the DA as a function of the main ring parameters, such as linear tunes, chromaticities, strength of the Landau octupoles, and phase advance between the two high–luminosity insertion regions, have been carried out. The dependence on the field quality of the main HL–LHC magnet families has been a major activity. In this respect, given that magnetic measurement results are becoming available, their impact on the DA has been assessed in detail, also in view of providing guidance to the magnets' acceptance process prior to installation in the tunnel (parenthetically, these intense tracking campaigns profited from the support of the volunteer–computing platform LHC@Home[89]). Of course, each configuration has been probed for both magnetic channels corresponding to the two beams. The ring configuration did not include the beam–beam effects and the target minimum DA has been set to 12 σ at injection and 10 σ at flat–top energy for the nominal HL–LHC emittance of 2.5 μm and a relative momentum deviation of 2.7×10^{-4}.[20] These values ensure that the impact of the magnets' field quality is in the shadow of that of the beam–beam effects (the target DA with beam–beam being around 6 σ, see next section). While at injection energy the field quality is fully compatible with the target DA, this is not completely the case at flat top

and special care has been taken to study and improve the way the non–linear corrector magnets should be operated. This topic is particularly challenging and and is discussed in more detail in Chapter 28.

5. Incoherent Collective Effects

5.1. *Beam–Beam*

The incoherent beam-beam interaction has been a limiting factor for the beam and luminosity lifetime of past and present colliders. In combination with machine imperfections, magnetic non–linearities and noise effects, it can limit the DA at collision and thereby impact performance by imposing limits on beam brightness (in particular due to the head-on effect) or on the minimum normalized BBLR separation. Although in the HL–LHC, the crossing angle impact to the virtual luminosity is mitigated by the crab crossing, a reduced crossing angle is always beneficial for reducing the requirements on insertion magnets' aperture, the irradiation of the triplet magnets by luminosity debris[90] and to maximize β^* reach.

The fact that the incoherent BBLR effects dominate the reduction of the DA at collision was evidenced since the design phase of the LHC.[47,91,92] Driven by beam dynamics considerations in LHC simulations,[93] the target value for the 10^6–turn minimum DA was chosen to be 6 σ for the nominal HL–LHC emittance of 2.5 μm and a relative momentum deviation of 2.7×10^{-4}.[94] An experimental analysis of the observed beam lifetime has been initiated since LHC Run 1.[95] A clear demonstration of the correlation between beam lifetime and DA at collision was provided during Run 2.[96–100] In Figure 5, the simulated minimum DA (over a set of initial transverse amplitude ratios) and the measured burn–off corrected lifetime (in logarithmic scale) during crossing angle reduction experiments is being presented for two type of beams (BCMS in orange and "8b+4e" in blue).[96,101] The beam lifetime after subtraction of the luminosity burn–off must be significantly larger than the burn-off lifetime to minimize the impact of the DA reduction due to non-linearities at collision. For example, a burn–off corrected lifetime 10 times longer than the burn-off lifetime will reduce the total beam lifetime by 10%. Therefore DA limits should be set to guarantee a burn-off corrected lifetime of a few hundred hours taking into account that the burn–off beam lifetime ranges between 10

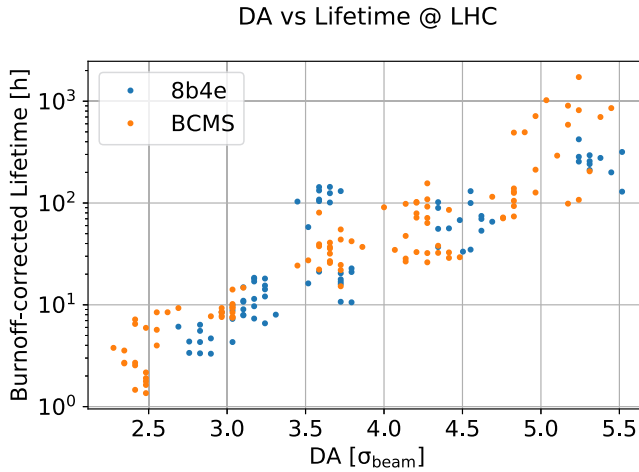

Fig. 5. Measured burn–off–corrected lifetime plotted against the corresponding simulated DA along two MD fills for crossing angle reach studies, for BCMS (orange) and "8b+4e" (blue) beam types.[96,101]

and 20 h during the fill for the HL-LHC nominal scenario with two high luminosity IPs. A minimum DA of 6 σ (or 5 σ in the presence of magnetic field errors) is therefore mandatory also to account for additional effects that cannot be simulated yet (e.g. as the impact of electron cloud (e–cloud) on lifetime observed at the end of Run 2[98,99]).

Multi–parametric DA studies have validated the operational scenario[7] both for nominal and ultimate luminosity with a constant half crossing angle of 250 μrad in IP1 and IP5, including the margins for reducing it during the collision process, through working point (WP) optimisation.[97,102,103] In Figure 6, DA tune scans at the start (top) and at the end (bottom) of the levelling process are presented, with the black lines representing to iso–DA contours. The Landau octupoles are powered at -300 A (i.e. at approximately half of their maximum current) and partially compensate the BBLR tune-spread,[104,105] whereas the chromaticity is set to 15 units. Adjusting the WP to (62.315, 60.320) at the end of levelling is crucial for guaranteeing DA of 6 σ (bottom), leaving very little margin for further optimisation. Although at the start of levelling (top) there is more margin with respect to DA, because of the large head-on tune-spread the optimal WP is found at (62.320, 62.325). This means that the WP should be varied along the diagonal during the levelling process,

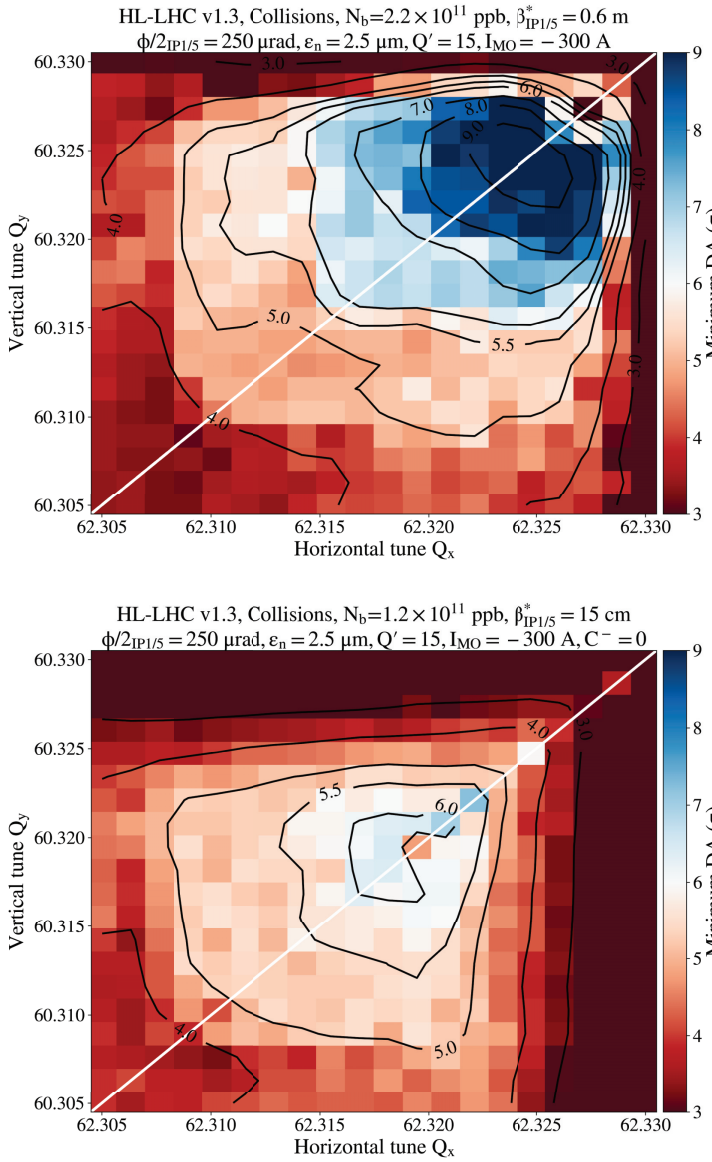

Fig. 6. DA tune scans at the start (2.2×10^{11}ppb, top) and the end of levelling (1.2×10^{11}ppb, bottom), at a half crossing angle of 250 μrad with octupoles at -300 A and chromaticity of 15 units. No field errors have been considered here.[97,102,103]

even if the crossing angle is kept constant during the fill, a complication that could be solved with additional non-baseline measures such as the BBLR compensation with DC wires (see Chapter 27).

The correlation of the (half) crossing angle with the bunch population in terms of DA at $\beta^* = 15$ cm and the optimised working point is shown in the top part of Figure 7. On top of the iso-DA lines, the iso-luminosity contours are overlayed in units of 10^{34} cm^{-2}s^{-1}. The 6 σ DA with a constant half crossing angle of 250 μrad and target luminosity of 5×10^{34} cm^{-2}s^{-1} can be maintained until the intensity drops to around 1.2×10^{11} ppb, through the above-mentioned WP optimisation. At the ultimate luminosity of 7.5×10^{34} cm$^{-2}s^{-1}$, and for the same crossing angle, the DA is slightly below 6 σ. Operation at high luminosity of LHCb (1.5×10^{34} cm^{-2} s^{-1}) appears to be also compatible with the above DA target, although it might limit the possibility of further optimizing the crossing angle throughout the levelling phase by reducing it further, for $\beta^* > 15$ cm, up to a target DA (adaptive crossing angle scenario).[9,97,102,103] The impact of magnetic field imperfections is presented in the bottom part of Figure 7, where DA simulations are performed assuming 60 different realizations of the machine. A statistical analysis is performed for the nominal (blue) and ultimate (red) luminosity operation. The average DA spread is found to be at the level of 0.3 σ. Therefore, the beam–beam interaction is the main DA degradation mechanism, while the magnetic imperfections have a minor additional effect. It should be stressed that even for the worst seed, a 5 σ DA can be guaranteed.

The interplay between the non–linearity of the beam—beam interaction with machine non-linearities and various sources of noise can further enhance diffusion, thereby leading to emittance blow-up and beam losses. The main sources of noise studied for the HL-LHC is the ripple in the phase and amplitude of crab cavities voltage and in the current of magnet power converters. The white random phase noise in the crab cavities can be efficiently suppressed by the transverse feedback (ADT) with a damping time of 10 turns.[106,108–110] The crab cavity relative voltage amplitude noise is estimated as 5×10^{-5},[106] causing a luminosity loss of about 2%[107] for both nominal and ultimate scenarios. From measurements during the crab cavity prototype tests in the SPS it was initially expected that the HL-LHC emittance growth estimates would be too pessimistic.[111] However recent studies show that the emittance growth suppression in the SPS is due to collective effects only appearing in

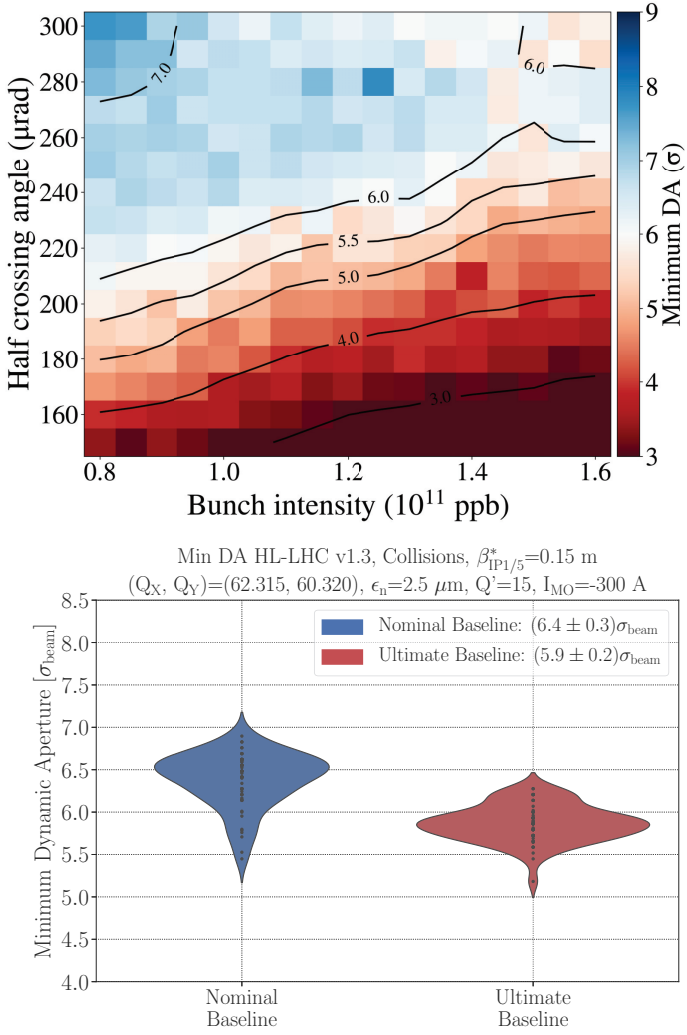

Fig. 7. DA correlation of half crossing angle and bunch population towards the end of levelling (top) and statistical result of the impact of magnetic field imperfections in DA for the nominal (blue) and ultimate (red) scenario at the end of levelling (bottom).[97,102,103]

the SPS[112] and therefore not relevant for HL-LHC. The only hope to mitigate the emittance growth from crab cavity amplitude noise in the HL-LHC is via a dedicated feedback, not foreseen in the project baseline.

The requirements for magnet power supply current noise have been studied for low[50,54] and high-frequencies.[113] The observations in the present LHC of noise spectral lines at around 8 kHz is of concern. A simulation and measurement campaign to clearly identify its origin and impact on DA and thereby lifetime is presently undertaken.[113,114]

5.2. *Emittance degradation mechanisms*

The emittance evolution in the present LHC is dominated by IBS, electron cloud, noise, synchrotron radiation (at flat top) and some additional mechanisms yet to be fully identified.[98,115,116] A model for the emittance evolution based on semi-analytical IBS models including coupling and a numerical parametrisation of growth rates for all possible dependent parameters has been built and was used as a tool to identify instrumentation issues and follow-up luminosity performance during Run 2,[117,118] coupled with a fully automated numerical framework for data monitoring and off-line analysis. This model, in combination with the measured data in particular during the last year of Run 2, was then used to estimate HL–LHC performance.[115] For the nominal and the ultimate scenarios, the extra transverse emittance growth at collisions results in a 2% degradation of the integrated luminosity per day (additional to the CC noise contribution).

6. Beam Induced Heat Loads on Cryogenic Beam Screens

The LHC and HL–LHC cryogenic magnets are equipped with actively cooled beam-screens, which intercept beam induced heating mainly due to synchrotron radiation, impedance and e-cloud effects.[47] The nominal operating temperature is 20 K for most of the beam screens, with the exception of the new inner triplet assemblies and the D1 dipoles in IR1 and IR5, which will be operated at higher temperature (60 - 80 K).

Large heat loads on the beams screens have been observed during the LHC Run 2, when the LHC was routinely operated with the 25 ns bunch spacing, as assumed in the LHC design and in the the HL–LHC baseline.[119,120] Figure 8 (left) shows the heat loads measured in the LHC arcs during two consecutive fills in 2017. The first is a regular physics fill using the 25 ns bunch spacing and a bunch population of 1.1×10^{11} p/bunch, while the second is a

test fill performed with the same bunch population but with a bunch spacing of 50 ns. It can be noticed that, with the 25 ns spacing, the heat loads are much larger than expected from impedance and synchrotron radiation and, in some of the arcs, are very close to the design cooling capacity of 160 W/half-cell (corresponding to 8 kW/arc). With the 50 ns, instead, the heat loads are much smaller and compatible with the expectation from impedance and synchrotron radiation. Moreover, with the 25 ns, beams large differences are observed among the eight LHC arcs. These differences are unexpected as the arcs are by design identical, and their origin is presently being investigated.[120,121]

Such a large difference between fills performed with different bunch spacings, together with other experimental observations with different beam conditions, allow excluding that the observed differences among sectors are originated by an artefact in the cryogenic measurement and point to e-cloud effects as the only plausible cause.[122]

Figure 8 (right) shows the estimated heat loads on the arc beam screens as a function of the bunch population for one of the sectors having the largest heat load.[123] The contributions from different sources are indicated with different colours. The e-cloud contributions are calculated inferring the Secondary

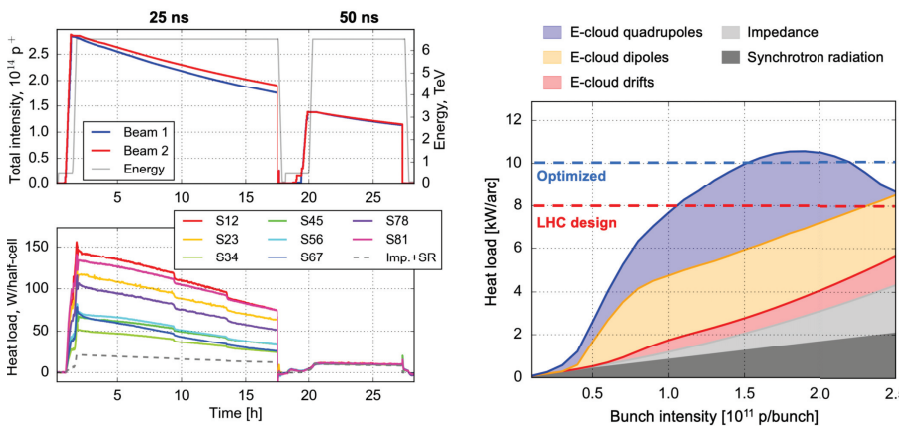

Fig. 8. Left: Heat loads measured during a regular luminosity fill with 25 ns bunch spacing and during a subsequent test fill with 50 ns bunch spacing, both with 1.1×10^{11} p/bunch. Right: Heat load expected for the sector showing the highest load (S81) as a function of the bunch population. The different contributions are indicated in different colors. The cooling capacity for the LHC design and the optimized cryogenics configuration is shown by the dashed lines.

Electron Yield (SEY) of the beam screen surface from the heat loads measured during LHC operation and assuming that this will remain unchanged (after conditioning) in the HL–LHC era.

The increase in bunch population, from 1.1×10^{11} p/bunch presently used at the LHC to 2.3×10^{11} p/bunch foreseen for HL–LHC, implies a significant increase in the contributions from impedance and synchrotron radiation. Nevertheless, only a relatively mild increase of the total heat loads is expected for bunch intensities above 1.2×10^{11} p/bunch, due to the fact that the contributions from e-cloud are not expected to increase significantly for larger bunch population.

The red line in Figure 8 (right) represents the available cooling capacity for the arc beam screens in the design configuration of the LHC cryogenics.[47] This would not be sufficient to cope with the expected heat loads. During Run 2, the LHC cryogenics has been operated in an optimized configuration (using one cold-compressor unit to serve two consecutive sectors) profiting from the lower-than-expected heat loads at 1.9 K. The compatibility of this optimized configuration with the HL–LHC operational scenarios is being verified. With this optimized configuration, a higher cooling capacity becomes available for the arc beam screens,[124] as indicated by the blue line in Figure 8 (right), which is very close to the maximum load expected during the HL–LHC luminosity fill.

The dependence of the e-cloud heat load on the bunch population is a critical input for the estimates made above, which were based on numerical simulations of the e-cloud buildup. Direct experimental checks of these simulation results were not possible in Run 2 using long bunch trains for intensities above 1.2×10^{11} p/bunch, due to intensity limitations in the injectors. Nevertheless, towards the end of 2018, trains of 12 bunches with high bunch population (up to 1.9×10^{11} p/bunch) became available from the injectors and could be used for tests in the LHC. The results of those experiments are shown in Figure 9 (left). The data clearly show that the heat loads from e-cloud tend to saturate above 1.5×10^{11} p/bunch. When comparing the measurement results against simulations, very good agreement is found especially for the high-load sectors, as shown in Figure 9 (right).[123]

The beam screen in the new magnetic elements developed for HL–LHC will receive a surface treatment (coating with amorphous carbon) to reduce the surface SEY and suppress the e-cloud.[125,126] The treatment will be applied

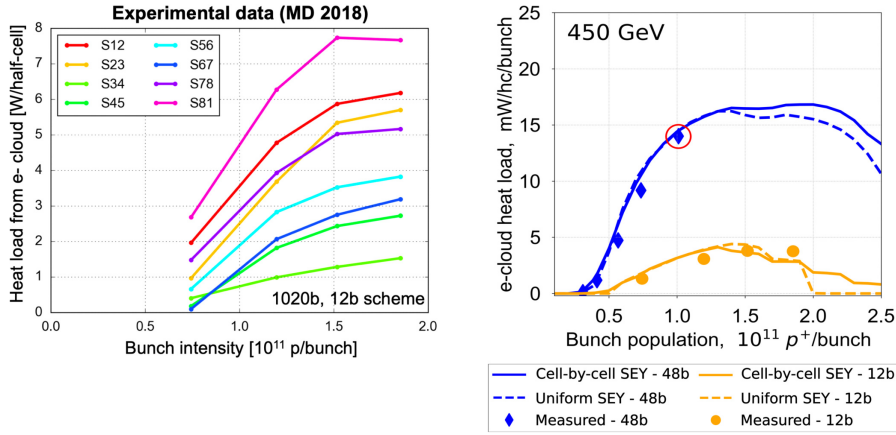

Fig. 9. Left: Heat loads measured for different bunch intensities at 450 GeV in the eight LHC arcs using trains of 12 bunches. The load expected from impedance and synchtrotron radiation is subtracted. Right: Comparison of simulation results against measured heat-load data for one of the sectors showing the highest heat load. The continuous line is calculated assuming different SEY in the different half-cells. The dashed line is based on a simplified model assuming uniform SEY over the entire arc. The data point used to infer the SEY values is circled in red.

also on critical elements already present in the LHC, in particular all the inner triplets and some of the matching quadrupoles in IR1, IR2, IR5 and IR8.

In case the intensity limitations from the heat loads on the beam screens are found to be stronger than expected, the heat loads can be mitigated exploiting the flexibility in the filling pattern design. A reduction of the heat loads by about 8% can be achieved using trains of 48 bunches instead of trains of 72 bunches, with practically no impact on the number of circulating bunches.[127] A stronger reduction of the heat loads can be achieved exploiting the "8b+4e" filling pattern made of short trains of 8 bunches separated by gaps of 4 empty slots. With this scheme the number of circulating bunches is reduced to 1972 bunches per beam. Hybrid schemes mixing standard and "8b+4e" bunch trains can also be envisaged, which allow maximizing the number of bunches, compatibly with the available cooling capacity.[128] The effectiveness of the "8b+4e" scheme for electron cloud suppression as well as that of the hybrid schemes have been proven experimentally in the LHC.[123,129]

7. Coherent Collective Effects

7.1. *The HL–LHC impedance*

The current HL–LHC impedance model has been constructed by adding the contributions of the main accelerator components interacting with the beam, mainly from analytical models and simulations.[130] The relative contributions of the different equipment to the transverse (dipolar) and longitudinal impedance models are plotted for 1 kHz to 10 GHz at top energy (for the pre-squeeze at $\beta^* = 50$ cm) in Figure 10 (the impedance model at injection energy can also be found in[130]). The LHC effective impedance is significant at high energy, when the primary (TCP) and secondary (TCSG) collimators in the betatronic collimation section in LSS7, become its dominant contributors, over a wide range of frequencies, because of their small gaps. As the impedance is composed of several complex functions of frequency, it is not possible to represent the impedance by a single number to have an idea of the importance of the collimators. Instead, what can be done is to look at the Landau octupole current required to stabilise the HL-LHC beam at 7 TeV for the assumed chromaticity and transverse damper gain (the Landau octupole current, the chromaticity and transverse damper are the three knobs available in the LHC and HL-LHC to stabilise the transverse coherent instabilities, as discussed in more detail below). It can be seen in particular that 98% of the required Landau octupole current is coming from the collimators and that the IR7 collimators alone (both primaries and secondaries) contribute to 79%.[130] During Run 2, systematic measurements have been performed to characterize the present LHC impedance model for both beams in both planes. These are in agreement with expectations, with an uncertainty that is estimated to be less than 50%.[131,132]

The expected strength of the Landau octupoles corresponding to the onset of transverse instabilities is in good agreement with observations[133] but only when stability is considered on short time scales (shorter than few minutes). For longer time scales, typical of transition times between different phases of the cycle, noise sources acting on the beam and inducing dipolar oscillations at the level of $10^{-4}\ \sigma$ (with σ being the rms beam size) are observed to affect beam stability at approximately twice the threshold Landau octupole strength. The origin of this noise and the mechanisms leading to transverse instabilities

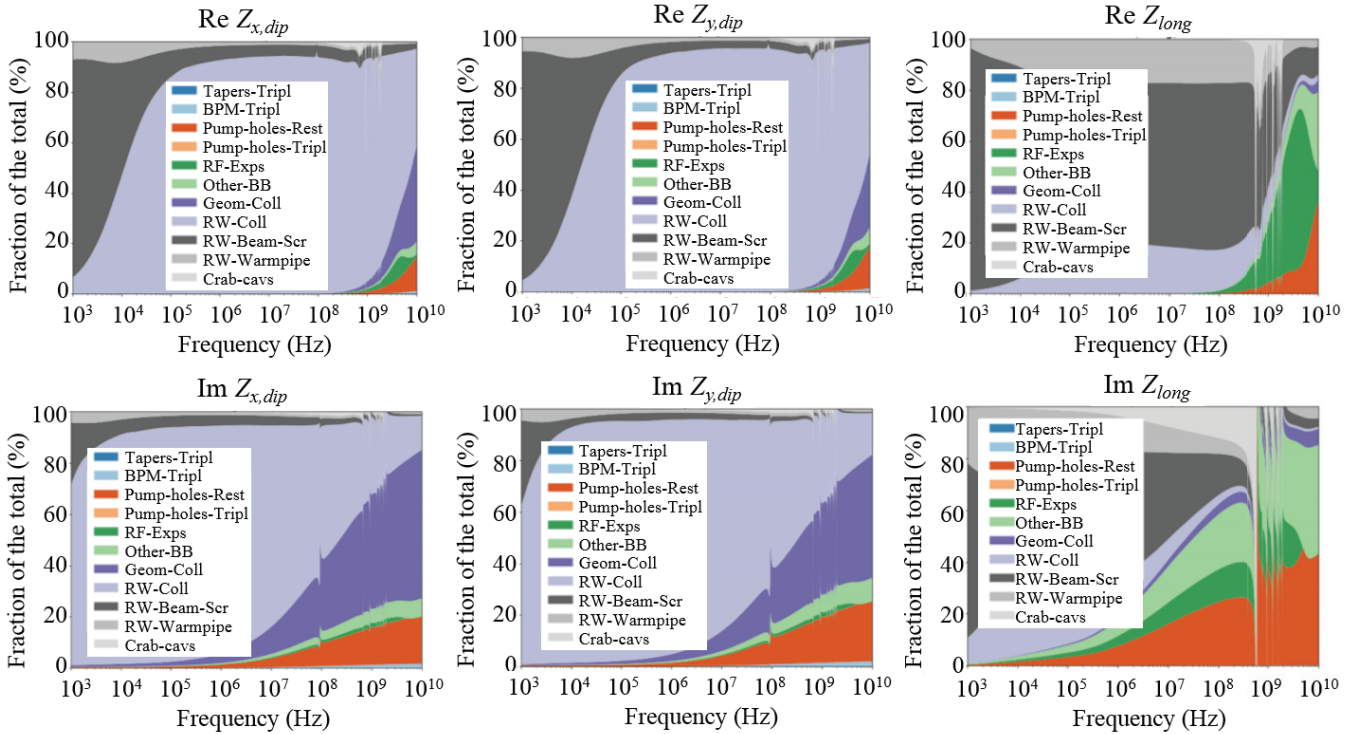

Fig. 10. Relative impedance contributions of the different considered elements to the total HL–LHC impedance at top energy (for the pre-squeeze at $\beta^* = 50$ cm) as a function of frequency (left: horizontal, middle: vertical, right longitudinal - top: real, bottom: imaginary).

are being investigated in detail (see Chapter 29) as a possible explanation of the above discrepancy.

New low-impedance collimators will be installed to replace and enhance, with the addition of embedded beam position monitors, the functionality of the existing ones:,[20,134] 2 Molybdenum-Graphite (MoGr) primary collimators per beam (TCPPM) and up to 9 Molybdenum coated (5 μm coating thickness) MoGr secondary collimators per beam will be installed. A significant effort has also been put in maintaining a low geometric impedance of the collimators by optimizing their design.

The impedance reduction with Mo-coated MoGr collimators has been tested and validated through extensive laboratory and beam-based measurements.[131,135] In addition, attention must be paid to the impedance of new pieces of equipment, in particular for those being installed in regions with high β functions (e.g. crab cavities), which are enhancing the effects of transverse impedance. For the crab cavities, a limit of 1 MΩ/m on the transverse shunt impedance of each High–Order Mode (HOM) has been chosen as a guideline to avoid that this equipment visibly affects the corresponding stability thresholds expressed by the additional Landau octupole strength required to stabilize the corresponding transverse instabilities.[136] The HOMs, whose frequencies are potentially dangerous for beam induced heating and have to be closely monitored during production, have been identified taking into account recent tests at SPS.[137–139] An overall description of the studies carried out, of the design guidelines provided and actions taken is available in Ref. [130].

The major beam induced RF heating issues that occurred in the first years of high intensity LHC operation were efficiently tackled with the help of the respective equipment groups (see Table 20 of Ref. [130]). The main showstoppers to reach the HL–LHC intensity were identified as the extra beam screen heat load due to e-cloud (see Section 6) and the injection kicker (MKI) operating temperature limit (for which a new design is being studied to reduce the temperature increase of the ferrite core).[130,140] The design of the new Injection Absorber (TDIS) includes an adequate cooling system to cope with the expected deposited power.[130,141] With the increase of bunch intensity, other devices may heat up beyond their acceptable limit and this is why all available temperature probes are carefully followed up during the run for signs of issues. Additional monitoring is recommended wherever possible.

7.2. *Beam stability*

Three main mitigation methods exist for both LHC and HL–LHC to stabilize the beam transversally: (i) Landau octupoles, with a possible boost from the ATS optics; (ii) chromaticity and (iii) transverse damper. The first mitigation method, Landau damping, is a general physical process that arises when a collection of particles, which have a spectrum of resonant frequencies, is considered and interact in some way. In particle accelerators we are usually concerned with an interaction that makes the beam unstable (due to the impedance for instance) and we want to find out whether or not the spread of resonant frequencies will stabilise it. Indeed, if the particles have a spread in their natural frequencies, the motion of the particles can lose its coherency and the beam can be stabilised. The Landau octupoles are used to generate this spread through amplitude detuning. For HL-LHC, the frequency spread can be increased thanks to the ATS optics, which increases the effect of the Landau octupoles by increasing the beta function at their location. The second mitigation method, chromaticity (which is modified through sextupoles), shifts the beam spectrum with respect to the impedance and therefore modifies the interaction between the beam and the impedance and the associated instabilities. Finally, the third mitigation method, transverse damper, is an electronic device which first detects the motion of the beam at some location (with a beam position monitor) and then kicks the beam to put it back on the design orbit (with a kicker magnet): it can be seen as a kind of negative impedance.

However, these three methods can have detrimental effects on the dynamic aperture and beam lifetime and a trade-off needs to be found: the value and sign of both the current in the Landau octupoles and chromaticty need to be optimised as well as the gain, the bandwidth and the noise of the transverse damper. From the LHC design report,[47] it was clear that due to the huge impedance produced by the collimators, transverse beam stability at high energy would require the use of chromaticity, or transverse damper, or both, as the octupole current alone would not be enough to stabilize the beam.[47,131]

The scenarios for operation at nominal and ultimate luminosity are described in Ref. [7] and they take into account the experience gained during Run 1 and Run 2.[142–146] The following effects have been or are gradually being taken into account: beam coupling impedance, electron cloud, head-on and long-range beam-beam forces, realistic transverse feedback and machine opti-

cal parameters like tunes, linear coupling,[147] linear and non-linear chromaticity, Landau octupole strength and other non-linearities and, more recently, the effect of noise[144,148] (see Chapter 29). However, about a factor 2 stronger Landau octupoles are still required as compared to expectations. Several investigations are ongoing to further reduce all the uncertainties of the model: (i) interplay of noise, transverse damper and impedance, (ii) better impedance model and (iii) understanding discrepancies at low chromaticity.[149] Potential additional mitigation paths are being analysed: modifying IR7 optics to reduce the effective collimator impedance and using asymmetric collimation schemes.[131] The baseline scenario provides stability with margin dictated by the present experience compatibly with sufficient dynamic aperture[131] (see Figure 11, where the required relative increase of the peak beta functions induced in the arcs with the ATS optics, called telescopic index or tele-index, are specified for both Landau octupoles polarity).

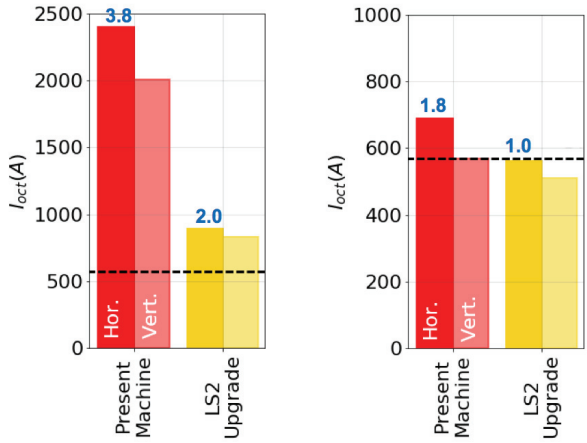

Fig. 11. Required Landau octupole current to stabilise the beam in the presence of both impedance (for the horizontal and vertical planes, with the present and HL–LHC LS2 upgrade cases) and beam-beam effects and for the most stringent scenario going in collision to produce the ultimate luminosity: (left) for the negative sign of the Landau octupole current and (right) for the positive sign of the Landau octupole current. The numbers in blue indicate the required boost from the ATS optics, i.e. the required tele-index, which describes the relative increase of the peak beta functions induced in the arcs, to achieve stability while keeping the octupole current at its maximum (570A, black line). These values have been obtained by considering a factor two in the required Landau octupole current, based on the LHC experience in 2018.[131]

The operation with 25 ns beams relies heavily on beam-induced scrubbing and the pace of the intensity ramp-up after the Long Shut-Down 2013-2014 (LS1) (when practically all LHC beam screens and vacuum chambers were vented to air for interventions) has been determined by electron cloud effects both from the heat load and beam stability points of view,[150,151] as expected. Although a significant reduction of the SEY has been obtained during Run 2 through scrubbing, significant differences in the final value of the SEY, inferred from measurements of the heat load, have been observed in different sectors, in different cryogenic cells and in different magnets within the same sector and cryogenics cell, respectively[119,122] (see Section 6). Coherent beam instabilities are expected and observed[144,152] in the LHC at injection as a result of the residual electron cloud, in particular in the quadrupoles. Machine settings with high chromaticity and Landau octupoles[7] are considered to be sufficient to stabilize the HL–LHC beam taking into account the non-monotonic dependence of the electron cloud density as a function of the bunch population.[120,153,154] However, these settings will have a stronger impact on the DA compared to the LHC.[155] Simulation studies are ongoing in order to identify the optimal configuration, which will be experimentally tested during Run 3. Transverse coupled-bunch instabilities driven by e-cloud effects could be simulated recently for the first time at CERN on a High Performance Computing cluster after parallelization of the simulation codes.[156] Detailed analyses and scans at injection are ongoing.

Amorphous carbon (a-C) coating of the beam screens of the superconducting magnets together with the non-monotonic dependence of the electron cloud density in the arcs on the bunch population should prevent electron cloud instabilities at high energy after scrubbing and in particular at the higher bunch populations.[126] Instabilities driven by e-cloud[153,154] could be observed in LHC at the end of long physics fills (so-called "pop-corn instabilities") due to the increase of electron density in the centre of the dipole magnets. If this occurs, the beams can be stabilized by increasing the chromaticity up to 15-20 units. Note that the a-C coating is expected to have a negligible effect on the overall machine impedance and related effects.[157]

The longitudinal beam parameters of the HL–LHC beams in collision described in Ref. [7] for the various phases of the HL–LHC cycle, have been updated with respect to those listed in Ref. [9] to guarantee the longitudinal beam stability.

7.3. *Beam-beam coherent effects*

The higher bunch population and lower β^* required in HL–LHC as compared to LHC imply stronger beam-beam interactions. The bunch-to-bunch differences introduced by missing beam-beam interactions, so-called PACMAN effects, were studied for the LHC and determined to not affect its performance.[158,159] They generate bunch–to–bunch orbit, tune and chromaticity offsets that were re-assessed for HL–LHC, with emphasis on the impact on physical aperture, beam loading on crab cavities, single particle and coherent stability of the beam. The new concept of PACMAN linear coupling driven by skew long-range beam-beam interactions was also introduced and implemented in the self-consistent code TRAIN,[160] adapted to the HL–LHC layout and optics.

Orbit, tune and chromaticity effects due to head-on and long-range beam-beam interactions are tolerable without dedicated mitigation measures in the nominal and utlimate scenarios.[161,162] Although small PACMAN orbit effects are not negligible (0.1 σ) and should be included in the definition of the aperture requirements, the luminosity loss due to the PACMAN orbit effects was shown to be negligible (of the order of 0.1%) in the high luminosity experiments and tolerable (i.e. smaller than the luminosity variation from intensity and emittance bunch to bunch fluctuations of the order of 10%) in the low luminosity ones. Nevertheless, the PACMAN orbit effect has an indirect impact on the long term stability of single particle trajectories since it imposes that the PACMAN bunches collide with a small offset, which modifies the non-linear forces that they experience at the IP. Linear coupling (driven by skew long-range beam-beam interactions) imposes tight tolerance on the alignment of the crossing angles bumps in the different IPs and its control will rely on measurement and correction of the orbit in the interaction region. Indeed, the PACMAN coupling generated by the combination of the crossing angle, the parallel separation bump and the orbit effects resulting from beam-beam long-range interaction at the opposing interaction region is already at the edge in terms of its detrimental effect on Landau damping (a maximum global coupling, described by the closest tune approach, of the order of 0.001 is recommended for the operational scenarios).

When operating with low β^*, or large crossing angles, or both, head-tail oscillations affect significantly the coherent forces between the beams. This mechanism allows for high-order mode-coupling instability of collid-

ing beams. The transverse damper, whose bandwidth limits its action to a constant kick over the bunch, is mostly efficient against the mode-coupling instability of low-order modes.[163] Numerical simulations accounting for the three-dimensional interaction of the two beams at the IPs for thousands of turns revealed that Landau damping by synchrotron side-bands is sufficient to maintain the beam stability in the configurations anticipated for HL–LHC.[164] Such a heavy simulation campaign relied on the implementation of a new high-performance computing cluster allowing fast parallel computations.

8. Alternative and Potential Operational Scenarios

Various alternatives to the present baseline configuration with the aim of either improving the potential performance or providing options for addressing possible limitations or changes in parameters[165] are briefly described in the following sections and summarized in Figure 12.

8.1. *"8b+4e" and hybrid filling schemes*

This scheme highly suppresses the formation of the electron cloud as discussed in Section 6. The lower number of bunches of the "8b+4e" scheme implies a lower peak luminosity at the same number of pile-up events per crossing. The single bunch parameters evolve as for the baseline during the physics fill. Therefore integrated luminosity simply scales linearly with the number of bunches. To maximize luminosity it is possible to mix "8b+4e" and BCMS trains to adapt the heat-load to the available cryogenic power.

8.2. *Other filling schemes*

The number of bunches in the PS trains could be increased from 72 to 80 in order to increase the integrated luminosity without affecting longitudinal peak pile-up density, as defined in.[165] Various fillings schemes have been considered offering integrated luminosity increases between 1.9% and 6.8% for all IPs.[166] The implications for machine protection in the SPS and in the LHC injection transfer lines due to the larger number of bunches per injection (from 288 to 320) are being analyzed.

8.3. *Flat optics with crab cavities*

A flat optics might be used with β^* of 7.5 cm and 18 cm in the separation and crossing planes, respectively, to improve the performance. Possible limitations on β^* may appear if IP5 has a vertical crossing angle. A crossing angle of 11.4 σ could be reached at the end of the fill for bunch populations of 1.1×10^{11} p/bunch applying approximate scaling from DA studies.[103,167–169] It must be noted that this configuration has not been fully validated yet and the operation at ultimate luminosity might not be possible unless β^* is increased or beam-beam long-range compensation schemes are implemented (see Chapter 27). The performance for this configuration is shown in Figure 12 and it exceeds the HL–LHC nominal performance in terms of integrated luminosity.

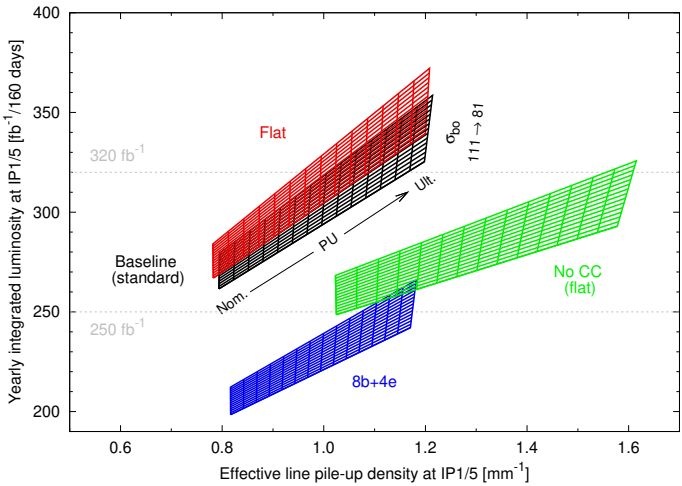

Fig. 12. Summary chart showing integrated luminosity per year versus effective pile-up density for the various scenarios considered. The impact of assuming less conservatively the effective cross section, from 111 mb to 81 mb for the estimate of the burn-off lifetime is also shown, indicating the importance of minimizing losses due to reduced DA and the potential gain in integrated luminosity.

8.4. *Flat optics without crab cavities*

Although crab-cavities have been successfully operated with beam in the SPS at reduced voltage, a back-up scenario has been developed in case of a major

crab cavity failure in HL–LHC. In this scenario, it is possible to partially recover the performance loss by resorting to flat optics with larger beam size in the crossing plane at the IP. The IP β functions that maximize luminosity are 7.5 cm and 31.5 cm. These β functions might not be possible if the IP5 crossing angle is in the vertical plane and an increase might be needed in this case. Also in this case beam-beam long range compensation schemes (see Chapter 27) might be required. Assuming flat optics in the absence of crab cavities reduces the performance by 5% in the nominal and 12% in the ultimate scenarios. The beam-beam long-range compensation could allow reducing the normalized long-range beam-beam separation from 12.6 σ to 11.0 σ improving the integrated luminosity from 249 fb^{-1} to 252 fb^{-1}.

References

1. ATLAS and CMS Collaborations, *Expected pile-up values at HL–LHC*, ATL-UPGRADE-PUB-2013-014, CERN (30 September 2013).
2. O.S. Brüning, *The High Luminosity LHC project*, in 6$^{\text{th}}$ Int. Particle Accelerator Conf. (IPAC 2015), Richmond, VA, USA, pp. 4096–4101.
3. L. Rossi and O.S. Brüning, *Progress with the High Luminosity LHC project at CERN*, in 10$^{\text{th}}$ Int. Particle Accelerator Conf. (IPAC 2019), Melbourne, Australia, pp. 17–22.
4. F. Zimmermann and O.S. Brüning, *Parameter Space for the LHC Luminosity Upgrade*, in Proc. 3$^{\text{rd}}$ Int. Particle Accelerator Conf. (IPAC'12), New Orleans, LA, USA, May 2012, paper MOPPC005, pp. 127–129.
5. D. Contardo, *private communication*, 3 December 2014.
6. F. Zimmermann, *HL–LHC: Parameter space, constraints & possible options*, LHC performance workshop, Chamonix 2011.
7. E. Métral *et al.*, *Update of the HL–LHC operational Scenarios for Proton Operation*, CERN-ACC-NOTE-2018-0002.
8. G. Arduini, O. Brüning, R. De Maria, R. Garoby, S. Gilardoni, B. Goddard, B. Gorini, M. Meddahi, G. Rumolo and R. Tomás Garcia, *Beam parameters at LHC injection*, CERN-ACC-2014-0006 (2014).
9. G. Apollinari *et al.* (ed.), *High-Luminosity Large Hadron Collider (HL–LHC): Technical Design Report V.0.1*, Geneva, Switzerland, Rep. CERN-2017-007-M, 2017.
10. W. Herr, B. Muratori, *Concept of luminosity*, CAS - CERN Accelerator School: Intermediate Course on Accelerator Physics, Zeuthen, Germany, 15–26 Sep 2003, CERN-2006-002, pp. 361–378.
11. O.S. Brüning, *HL–LHC parameter space and scenarios*, Proc. Chamonix 2012 Workshop on LHC Performance, Chamonix, France, 6–10 Feb 2012, Ed. C. Carli, CERN-2012-006 (2012), pp. 315–324.
12. V. Kain *et al.*, *Injection protection — Are we taking it seriously? How can we make*

it safer?, Proc. 2nd Evian Workshop on LHC Beam Operation, Evian, France, 7–9 December 2010, Ed. B. Goddard, CERN-ATS-2011-017, pp. 143–149.

13. R. Jacobsson, *Future wishes and constraints from the experiments at the LHC for the proton–proton programme*, ICFA Mini-Workshop on Beam–Beam Effects in Hadron Colliders (BB2013), CERN, Geneva, Switzerland, 18–22 Mar 2013, Eds. W. Herr and G. Papotti, CERN-2014-004 (2014), pp. 167–176.
14. E. Métral, *Pushing the limits: Beam*, Proc. Chamonix 2011 Workshop on LHC Performance, Chamonix, France, 24–28 January 2011, Ed. C. Carli, CERN-ATS-2011-005, pp. 252–260.
15. R.W. Assmann, *Implications of higher intensities in the LHC*, Proc. Chamonix 2011 Workshop on LHC Performance, Chamonix, France, 25–29 January 2010, Ed. C. Carli, CERN-ATS-2010-026, pp. 328–333.
16. H. Bartosik, G. Iadarola, Y. Papaphilippou, G. Rumolo and E. Shaposhnikova, *Can we ever reach the HL–LHC requirements with the injectors?*, Proc. Review of LHC and Injector Upgrade Plans Workshop, Archamps, 29–31 October 2013, Eds. B. Goddard, F. Zimmermann, CERN-2014-006, pp. 95–104.
17. S. Fartoukh and F. Zimmermann, *The accelerator physics challenges*, CERN-ACC-2014-0209 (2014) Advanced Series on Directions in High Energy Physics: Volume 24 (2015), World Scientific Chapter 4, pp. 45–96.
18. G. Arduini, R. Tomás Garcia, *HL–LHC Engineering Change Request — BEAM/ MACHINE PARAMETERS IN COLLISION* — UPDATE — LHC-_-EC-0039 v.1.0, EDMS 1908458.
19. HL–LHC Technical Coordination Committee Parameter Table v. 7.0.0 (18/03/2018). `https://espace.cern.ch/HiLumi/TCC/_layouts/15/WopiFrame.aspx?sourcedoc=/HiLumi/TCC/SiteAssets/HL_LHC_Parameter_Table.xlsx&action=default`
20. G. Apollinari *et al.* Eds., *High–Luminosity Large Hadron collider (HL–LHC) — Technical Design Report V 1.0*, to be published.
21. R. De Maria, *General method for final focus system design for circular colliders*, Phys. Rev. ST Accel. Beams **11**, p. 031001, 2008.
22. D. Gamba and R. De Maria, *IP Orbit Correction Update for HL–LHC*, in *Proc. 9th Int. Particle Accelerator Conf. (IPAC'18)*, Vancouver, Canada, Apr.-May 2018, pp. 3048–3051. `doi:10.18429/JACoW-IPAC2018-THPAF039`.
23. P. Baudrenghien and R. Calaga, *Update on CC RF noise and operational aspect*, presented at the 96th HiLumi WP2 Task Leader Meeting – Tuesday, 13 Jun. 2017, `https://indico.cern.ch/event/645814/`.
24. A. Herty *et al.*, *HL–LHC Full Remote Alignment Study*, presented at the 10th Int. Particle Accelerator Conf. (IPAC'19), Melbourne, Australia, May 2019, paper THPGW057.
25. R. De Maria, S. D. Fartoukh, A. V. Bogomyagkov, and M. Korostelev, *HLLHCV1.0: HL–LHC Layout and Optics Models for 150 mm Nb3Sn Triplets and Local Crab-cavities*, in Proc. 4th Int. Particle Accelerator Conf. (IPAC'13), Shanghai, China, May 2013, paper TUPFI014, pp. 1358–1360.
26. R. De Maria, S. D. Fartoukh, and M. Fitterer, *HL–LHCV1.1 Optics Version for the HL–*

LHC Upgrade, in *Proc. 6th Int. Particle Accelerator Conf. (IPAC'15)*, Richmond, VA, USA, May 2015, pp. 2090–2093. doi:10.18429/JACoW-IPAC2015-TUPTY037.

27. R. De Maria, R. Bruce, M. Giovannozzi, F. Plassard, and D. Gamba, *HL–LHC Optics and Layout V1.4*, presented at the 10th Int. Particle Accelerator Conf. (IPAC'19), Melbourne, Australia, May 2019, paper MOPMP019.
28. R. Bruce *et al.*, *Review of LHC Run 2 Machine Configurations*, in Proc. 9th LHC Operations Evian Workshop, Evian, Switzerland, January 2019.
29. R. Tomás *et al.*, *LHC Run 2 Optics Commissioning Experience in View of HL–LHC*, presented at the 10th Int. Particle Accelerator Conf. (IPAC'19), Melbourne, Australia, May 2019, paper MOPMP033.
30. X. Buffat *et al.*, *Transverse Instabilities*, in *Proc. 9th LHC Operations Evian Workshop*, Evian, Switzerland, January 2019.
31. R. De Maria *et al.*, *HLLHCV1.4 Optics repository*, http://lhc-optics.web.cern.ch/lhc-optics/HLLHCV1.4/.
32. J. Jowett, M. Schaumann and R. Versteegen, *Heavy-ion operation of HL–LHC*, in Adv. Ser. Dir. High Energy Phys. 24 (2015) pp. 359–371.
33. S. Fartoukh *et al.*, *Achromatic telescopic squeezing scheme and by-products: From concept to validation*, Phys. Rev. Accel. Beams **24**, 021002.
34. I. Efthymiopoulos *et al.*, *LHCb Upgrades and operation at* $10^3 4\ cm^{-2}\ s^{-1}$ *luminosity –A first study*, CERN-ACC-NOTE-2018-0038.
35. R. De Maria and M. Solfaroli, *Smooth and Beta-Beating-Free Optics Transitions for HL–LHC*, presented at the 10th Int. Particle Accelerator Conf. (IPAC'19), Melbourne, Australia, May 2019, paper MOPMP020.
36. S. Redaelli, *et al.*, *Plans for Deployment of Hollow Electron Lenses at the LHC for Enhanced Beam Collimation*, in Proc. 6th Int. Particle Accelerator Conf. (IPAC'15), Richmond, VA, USA, May 2015, pp. 2462–2465. doi:10.18429/JACoW-IPAC2015-WEBB1.
37. R. Bruce, *et al.*, *Reaching record-low* β^* *at the CERN Large Hadron Collider using a novel scheme of collimator settings and optics*, Nucl. Instrum. Methods Phys. Res. A, vol. **848**, pp. 19–30, 2017.
38. C. Bracco *et al.*, *Update on optics constraints for injection and dump protection elements*, presented at the 30th HL–LHC TCC meeting on 8 June 2017, https://indico.cern.ch/event/638356/.
39. R. Tomás, *et al.*, *Record low beta beating in the LHC*, Phys. Rev. ST Accel. Beams **15**, p. 091001 (2012).
40. E.H. Maclean, *et al.*, *New approach to LHC optics commissioning for the nonlinear era*, Phys. Rev. Accel. Beams **22**, 061004, 2019.
41. E.H. Maclean, *et al.*, *Detailed review of the LHC optics commissioning for the nonlinear era*, CERN-ACC-2019-0029.
42. F. Carlier, *et al.*, *Optics Measurement and Correction Challenges for the HL–LHC*, CERN-ACC-2017-0088.
43. J. Coello *et al.*, *MD2148: Flat optics*, CERN-ACC-NOTE-2018-0051.

44. R. Bruce, *et al.*, *Updated parameters for HL–LHC aperture calculations for proton beams*, CERN-ACC-2017-0051.
45. R. Tomás, *et al.*, *Review of linear optics measurement and correction for charged particle accelerators*, Phys. Rev. Accel. Beams, vol. **20**, p. 054801 (2017).
46. F. Carlier and R. Tomás, *Accuracy and Feasibility of the β^* Measurement for LHC and High Luminosity LHC using K-Modulation*, Phys. Rev. Accel. Beams **20**, 011005, Jan. 2017.
47. O. Brüning (ed.) *et al.*, *LHC Design Report*, Geneva, Switzerland, Rep. CERN-2004-003-V-1, Jun. 2004.
48. R. Carcagno, *Functional Specifications MQXFA Magnets*, CERN EDMS No. 1535430.
49. R. Carcagno, S. Feher, *Functional Specifications LMQXFA Cold Mass*, CERN EDMS No. 1686197, `https://edms.cern.ch/document/1686197`.
50. D. Gamba *et al.*, *Update of beam dynamics requirements for HL-LHC electrical circuits*, CERN-ACC-2019-0030.
51. M. Hofer, *et al.* , *K–modulation for future High energy colliders*, presented at the IPAC'19, Melbourne, Australia, May 2019, paper MOPMP022.
52. D.W. Wolf, "Analysis of tune modulations in the LHC", Bachelor thesis, CERN-THESIS-2018-251.
53. R. Tomás Garcia, *Trim in Q1 for the beta* measurements*, 27th Technical Coordination Committee, 30th March 2017, INDICO 590417.
54. D. Gamba *et al.*, *Beam dynamics requirements for HL–LHC electrical circuits*, CERN-ACC-2017-0101.
55. J. Coello *et al.*, *New local optics measurements and correction techniques for the LHC and its luminosity upgrade*, Phys. Rev. Accel. Beams **23**, 041001, April 2020.
56. M. Gasior, G. Baud, J. Olexa, and G. Valentino, *First Operational Experience with the LHC Diode ORbit and OScillation (DOROS) System*, in Proc. 5th Int. Beam Instrumentation Conf. (IBIC'16), Barcelona, Spain, Sep. 2016, pp. 43–46. `doi:10.18429/JACoW-IBIC2016-MOPG07`
57. A. Garcia-Tabares *et al.*, *Optics-measurement-based beam position monitor calibrations in the LHC insertion regions*, Phys. Rev. Accel. Beams **23**, 042801, April 2020.
58. E. Fol, R. Tomás and G. Franchetti, *Supervised learning-based reconstruction of magnet errors in circular accelerators*, The European Physical Journal Plus vol. **136**, Article number: 365 (2021).
59. E. Fol, R. Tomás, J. Coello de Portugal, and G. Franchetti, *Detection of faulty beam position monitors using unsupervised learning*, Phys. Rev. Accel. Beams **23**, 102805, 2020.
60. R. Tomás *et al.*, *LHC Run 2 Optics Commissioning Experience in View of HL–LHC*, presented at IPAC'19, Melbourne, Australia, May 2019.
61. M. Hofer and R. Tomás, *Effect of local linear coupling on linear and nonlinear observables in circular accelerators*, Phys. Rev. Accel. Beams **23**, 094001, 2020.
62. T. Persson, *et al.*, *LHC Optics Corrections in Run 2*, Proc. of 9$^{\text{th}}$ LHC Operations Evian Workshop, 2019, pp. 59–66.

63. D. Gamba, *Impact of flux jumps on orbit stability*, 150th HiLumi WP2 Meeting. `https://indico.cern.ch/event/823530/`
64. J. Coello *et al.*, *Impact of Flux Jumps in Future Colliders*, Phys. Rev. Accel. Beams **23**, 011001, January 2020.
65. N. M. Gelfand, *Calculations of the Dynamic Aperture at the Tevatron*, in Proceedings of SSC Workshop on Accelerator Physics Issues for a Superconducting Super Collider, edited by M. Tigner, UM-HE-84-1, 124, 1984.
66. V. Visnjic, *Dynamic aperture of low beta lattices at Tevatron collider*, in Proceedings of 1991 Particle Accelerator Conference, edited by J. Chew and L. Lizama (IEEE Computer Society Press, Piscataway - NY), 1701, 1991.
67. V. Visnjic, *Dynamic aperture of the future Tevatron Collider*, in Proceedings of Workshop On Nonlinear Problems In Future Particle Accelerators, edited by W. Scandale and G. Turchetti (World Scientific, Teaneck, NJ), 1991.
68. R. Brinkmann, F. Willeke, *Persistent Current Field Errors and Dynamic Aperture of the Hera Proton Ring*, DESY-HERA-88-08, 1988.
69. F. Zimmermann, F. Willeke, *Long term stability and dynamic aperture of the HERA proton ring*, DESY-HERA-91-08, 1991.
70. F. Zimmermann, *Dynamic aperture and transverse proton diffusion in HERA*, SLAC-PUB-6458, 1994.
71. O.S. Brüning *et al.*, *Comparison of measured and computed dynamic aperture for the SPS and the HERA proton ring*, Part. Accel. **54**, 223 (1996).
72. Y. Luo *et al.*, *Dynamic aperture evaluation at the current working point for RHIC polarized proton operation*, in Proceedings of 2007 Particle Accelerator Conference, edited by C. Petit-Jean-Genaz (IEEE Computer Society Press, Piscataway - NY, 2007), 4363, 2007.
73. E. Todesco and M. Giovannozzi, Phys. Rev. E **53**, 4067 (1996).
74. M. Giovannozzi, Phys. Rev. ST Accel. Beams **15**, 024001 (2012).
75. E.H. Maclean, M. Giovannozzi, and R.B. Appleby, *Innovative method to measure the extent of the stable phase-space region of proton synchrotrons*, Phys. Rev. Accel. Beams **22**, 034002 (2019).
76. E.H. Maclean, R. Tomás, F. Schmidt, and T.H. B. Persson, *Measurement of nonlinear observables in the Large Hadron Collider using kicked beams*, Phys. Rev. ST Accel. Beams **17**, 081002 (2014).
77. M. Giovannozzi, F. Van der Veken, *Description of the luminosity evolution for the CERN LHC including dynamic aperture effects, Part I: The model*, Nucl. Instrum. & Methods A **905**, 171.
78. M. Giovannozzi, F. Van der Veken, *Description of the luminosity evolution for the CERN LHC including dynamic aperture effects. Part II: application to Run 1 data*, Nucl. Instrum. & Methods A **908**, 1.
79. E. Todesco, M. Giovannozzi and W. Scandale, *Fast indicators of long-term stability*, Part. Accel. **55**, 273 (1995).
80. M. Giovannozzi and E. McIntosh, *Development of parallel codes for the study of nonlinear*

beam dynamics, Int. Jou. Mod. Phys. C **8**, 155 (1997).
81. M. Giovannozzi, W. Scandale, E. Todesco, *Prediction of long-term stability in large hadron colliders*, Part. Accel. **56**, 195 (1996).
82. M. Giovannozzi, W. Scandale, E. Todesco, *Dynamic aperture extrapolation in presence of tune modulation*, Phys. Rev. E **57**, 3432 (1998).
83. A. Bazzani, M. Giovannozzi, E.H. Maclean, C.E. Montanari, F.F. Van der Veken, W. Van Goethem, *Advances on the modelling of the time evolution of dynamic aperture of hadron circular accelerators*, submitted for publication (2019).
84. SixTrack web site: `http://cern.ch/sixtrack`
85. R. De Maria *et al.*, *SixTrack Version 5: Status and New Developments*, presented at the 10th Int. Particle Accelerator Conf. (IPAC'19), Melbourne, Australia, May 2019, paper WEPTS043.
86. A. Bazzani, O. Mazzarisi, M. Giovannozzi, E.H. Maclean, *Diffusion in stochastically perturbed Hamiltonian systems with application to the recent LHC dynamic aperture experiment*, in Nonlinear Dynamics and Collective Effects in Particle Beam, World Scientific, ed. by S. Chattopadhyay, M. Cornacchia, S. Di Mitri, p. 70.
87. A. Bazzani, M. Giovannozzi, E.H. Maclean, *Analysis of the CERN Large Hadron Collider non-linear beam dynamics at top energy by means of a new diffusion mode*, submitted for publication (2019).
88. Y. Cai, R. De Maria, M. Giovannozzi, Y. Nosochkov, F.F. Van der Veken, *Dynamic aperture studies for HL–LHC V1.0*, CERN-ACC-2018-0054 (2018).
89. J. Barranco, *et al.*, *LHC@Home: a BOINC-based volunteer computing infrastructure for physics studies at CERN*, Open Eng. **7**, 378 (2017).
90. F. Cerutti *et al.*, *Heat deposition and radiation dose vs operation mode and mitigation schemes*, Presentation in the LHC Performance Workshop 2018, 29 January – 1 February 2018, Chamonix, France. `https://indico.cern.ch/event/676124/contributions/2767903/`.
91. Y. Papaphilippou and F. Zimmermann, *Weak-strong beam-beam simulations for the Large Hadron Collider*, *Phys. Rev. ST Accel. Beams*, **2**, 104001, (1999). `https://link.aps.org/doi/10.1103/PhysRevSTAB.2.104001`.
92. Y. Papaphilippou and F. Zimmermann, *Estimates of diffusion due to long-range beam-beam collisions*, *Phys. Rev. ST Accel. Beams*, **5**, 074001, (2002). `https://link.aps.org/doi/10.1103/PhysRevSTAB.5.074001`.
93. Y. Luo and F. Schmidt, *Dynamic aperture studies for LHC optics Version 6.2 at Collision*, CERN LHC-Project-Note-310, (2003). `https://cds.cern.ch/record/692074`.
94. T. Pieloni, D. Banfi, and J. Barranco Garcia, *Dynamic Aperture Studies for HL–LHC with beam-beam effects*, May 2017. `https://cds.cern.ch/record/2263345`.
95. W. Herr, *et al.*, *Long range beam-beam effects*, in the LHC, Proc. ICFA Mini-Workshop on Beam-Beam Effects in Hadron Colliders, CERN, Geneva, Switzerland, 18–22 March 2013, Eds. W. Herr and G. Papotti, CERN-2014-004, pp. 87–92 (2014).
96. D. Pellegrini, *et al.*, *Incoherent beam-beam effects and lifetime optimization*, 8th Evian Workshop on LHC Beam Operation, Evian, France, 12–14 December 2017.

https://indico.cern.ch/event/663598/contributions/2782389/attachments/1574018/2521763/Pellegrini_Evian_Paper.zip.

97. Y. Papaphilippou, *et al.*, *Long range beam-beam effects for HL–LHC*, Presentation in the LHC Performance Workshop 2018, 29 January – 1 February 2018, Chamonix, France. https://indico.cern.ch/event/676124/contributions/2768610/.
98. S. Papadopoulou, *et al.*, *Transverse emittance blow-up*, 9th Evian Workshop on LHC Beam Operation, Evian, France, 30 January – 1 February 2019, INDICO: 751857.
99. S. Kostoglou,*et al.*, *Luminosity, lifetime and modelling*, 9th Evian Workshop on LHC Beam Operation, Evian, France, 30 January – 1 February 2019, INDICO: 751857.
100. K. Paraschou and G. Iadarola, *Status of the studies on Electron cloud incoherent effects*, 165th HiLumi WP2 Meeting.
101. H. Damerau, H. Bartosik, R. Garoby, S. Gilardoni, S. Hancock, B. Mikulec, Y. Papaphilippou, G. Rumolo, E. Shaposhnikova, R. Tomás, *LIU: Exploring Alternative Ideas*, Proc. Review of LHC and Injector Upgrade Plans Workshop, Archamps, 29–31 October 2013, Eds. B. Goddard, F. Zimmermann, CERN-2014-006, pp. 127–137.
102. N. Karastathis, *et al.*, *Refining the HL–LHC Operational Settings With Inputs From Dynamic Aperture Simulations: A Progress Report*, J. Phys.: Conf. Ser., **1067**, 022005, (2018). https://doi.org/10.108/1742-6596/1067/2/022005.
103. N. Karastathis, *et al.*, *Beam-beam simulation in the HL–LHC*, Presentation in the 8th HL–LHC Collaboration Meeting, 15–18 October 2018, CERN, Geneva, Switzerland. https://indico.cern.ch/event/742082/contributions/3085158/attachments/1736226/2808306/nkarast_HLCollab_18102018.pptx.
104. J. Shi, L. Jin and O. Kheawpum, *Multipole compensation of long-range beam-beam interactions with minimization of nonlinearities in Poincaré maps of a storage-ring collider*, Phys. Rev. E, **69**, 036502, (2004). https://link.aps.org/doi/10.1103/PhysRevE.69.036502.
105. J. Barranco Garcia and T. Pieloni, *Global compensation of long-range beam-beam effects with octupole magnets: dynamic aperture simulations for the HL–LHC case and possible usage in LHC and FCC*, May 2017. https://cds.cern.ch/record/2263347.
106. P. Baudrenghien, *Expected performances of the CC in terms of voltage and (phase) noise*, Presentation in the 96th WP2 Meeting, 13 June 2017, CERN, Geneva, Switzerland. https://indico.cern.ch/event/645814/contributions/2622537/attachments/1475139/2291022/Meeting_13_06_2017.pptx.
107. L. Medina *et al.*, *Effective pile-up density as a measure of the experimental data quality for High-Luminosity LHC operational scenarios*, CERN-ACC-2018-0003.
108. X. Buffat, *Emittance growth due to crab cavity noise and expected orbit spread at the crab cavity*, Presentation in the 96th WP2 Meeting, 13 June 2017, https://indico.cern.ch/event/645814/contributions/2622559/attachments/1475256/2284820/2017-06-13_CCnoise-offset.pdf.
109. J. Qiang, *et al.*, *Simulation of beam–beam interaction with crab cavities for LHC upgrade*, Nucl. Instrum. Methods Phys. Res., A, **900**, 53-59, (2018).
110. A. Alekou, *et al.*, *Deliverable 2.10: Summary of the observations in the SPS and update*

of the estimates for HL–LHC concerning phase and amplitude noise levels and RF multipoles, CERN-ACC-2020-0002.

111. P. Baudrenghien, *LLRF lessons learned from SPS tests, observed emittance growth*, Presentation in the 8th HL–LHC Collaboration Meeting, 15–18 October 2018, CERN, Geneva, Switzerland. https://indico.cern.ch/event/742082/contributions/3084929/attachments/1734377/2804529/HL--LHC18v5.pptx.
112. N. Triantafyllou et al, "New results of the SPS Crab Cavity noise emittance blow-up analysis", 187th HiLumi WP2 Meeting, February 2021.
113. S. Kostoglou, *et al.*, *Summary of observations on noise for LHC and projections for HL–LHC*, Presentation in the 63rd Technical Coordination Committee, 13th December 2018, CERN, Geneva, Switzerland. https://indico.cern.ch/event/779650/contributions/3244747/attachments/1770859/2877606/TCC_noise_131218.pptx.
114. S. Kostoglou, *et al.*, *An update on the LHC noise observations and studies*, Presentation in the Beam-Beam and Luminosity Studies meeting, 7 June 2019, CERN, Geneva, Switzerland. https://indico.cern.ch/event/817173/contributions/3445813/attachments/1858887/3054263/MD4147_BBLM_v1.0.pptx.
115. S. Papadopoulou, *et al.*, *Emittance growth in the LHC and impact on HL–LHC performance*, Presentation in the 8th HL–LHC Collaboration Meeting, 15–18 October 2018, CERN, Geneva, Switzerland. https://indico.cern.ch/event/742082/contributions/3085157/attachments/1736429/2808930/HILUMImeet_18102018_stef.pdf.
116. R. Tomás, J. Keintzel and S. Papadopoulou *Emittance growth from luminosity burn-off in future hadron colliders*, Phys. Rev. Accel. Beams **23**, 031002, March 2020.
117. F. Antoniou, G. Arduini, Y. Papaphilippou, and G. Papotti, *Building a Luminosity Model for the LHC and HL-LHC*, in Proc. 6th Int. Particle Accelerator Conf. (IPAC'15), Richmond, VA, USA, May 2015, pp. 2042–2045. doi:10.18429/JACoW-IPAC2015-TUPTY020.
118. F. Antoniou, *et al.*, *Can we predict luminosity*, in proc. of 7th Evian Workshop on LHC beam operation, Evian Les Bains, France, 2016. https://indico.cern.ch/event/578001/contributions/2366376/attachments/1388316/2222614/Evian2016_Lumi_F.Antoniou.pdf.
119. G. Iadarola, G. Rumolo, P. Dijkstal, L. Mether, *Analysis of the beam induced heat loads on the LHC arc beam screens during Run 2*, CERN-ACC-NOTE-2017-0066 (2018).
120. G. Iadarola, *et al.*, *Electron cloud and heat loads in Run 2*, in Proc. 9th LHC Operations Evian Workshop, Evian, Switzerland, January 2019.
121. L. Tavian, *Report from the task force on beam induced heat load*, presented at the LHC Performance Workshop 2018, CERN, 31 Jan 2018, https://indico.cern.ch/event/676124.
122. G. Iadarola, *e-cloud and heat load in the LHC arcs*, presented at the Accelerator and Beam Physics Forum, CERN, Geneva, Switzerland, Jul. 2018, https://indico.cern.ch/event/740046/.

123. G. Skripka, *Scaling of e-cloud effects with bunch population*, presented at the 143th HiLumi WP2 Meeting, CERN, Geneva, Switzerland, Mar. 2019, https://agenda.infn.it/event/13351.
124. K. Brodzinski, *Measurement of available beam screen cooling capacity on cryoplants*, presented at the LHC Machine Committee, CERN, 10 Apr 2019, https://indico.cern.ch/event/812689/
125. G. Skripka, G. Iadarola, *Beam-induced heat loads on the beam screens of the inner triplets for the HL–LHC*, CERN-ACC-NOTE-2018-0009 (2018).
126. G. Iadarola, E. Métral, G. Rumolo, *Beam induced heat loads on the beam screens of the twin-bore magnets in the IRs of the HL–LHC*, CERN-ACC-2016-0112 (2016).
127. G. Iadarola, *Heat-Load budget in the arcs at 7 TeV*, presented at the LHC Run-III Configuration Meeting, CERN, 22 Jun 2018, https://indico.cern.ch/event/732916.
128. G. Iadarola, *Digesting the LIU high brightness beam: is this an issue for HL–LHC?*, presented at the LHC Performance Workshop 2018, CERN, 31 Jan 2018, https://indico.cern.ch/event/676124.
129. G. Iadarola, *et al.*, *MD421: Electron cloud studies on 25 ns beam variants (BCMS, 8b+4e)*, CERN-ACC-NOTE-2017-0028 (2017).
130. D. Amorim *et al.*, *HL–LHC impedance and related effects*, CERN-ACC-NOTE-2018-0087.
131. E. Métral *et al.*, *Impedance models, operational experience and expected limitations*, International Review of the HL–LHC Collimation System, CERN, 11-12/02/2019.
132. D. Amorim *et al.*, *Comparison of LHC impedance model predictions to beam-based measurements*, 169th HSC section meeting, CERN, 18/02/2019.
133. L. Carver *et al.*, *Current status of instability threshold measurements in the LHC at 6.5 TeV*, in Proc. 7th Int. Particle Accelerator Conf. (IPAC'16), Busan, South Korea, May 2016, pp. 1434–1437. CERN-ACC-2016-234.
134. S. Antipov *et al.*, *Staged implementation of low-impedance collimation in IR7: plans for LS2*, CERN-ACC-2019-0001.
135. S. Antipov *et al.*, *Single-collimator tune shift measurement of the three-stripe collimator at the LHC*, in Proc. 9th Int. Particle Accelerator Conf. (IPAC'18), Vancouver, BC, Canada, May 2018, pp. 3036–3039. doi: DOI: 10.18429/JACoW-IPAC2018-THPAF035.
136. S. Antipov *et al.*, *Effect of crab cavity high order modes on the coupled-bunch stability of High-Luminosity Large Hadron Collider*, Phys. Rev. Accel. Beams **22**, 054401 (2019).
137. F. Giordano and B. Salvant, *Update on crab cavity beam induced heating*, 127th HSC section meeting, CERN, 20/11/2017.
138. S. Antipov *et al.*, *Update on beam stability due to HOMs and beam induced heating reflecting the recent changes in RFD crab cavity*, 129th HSC section meeting, CERN, 04/12/2017.
139. S. Antipov *et al.*, *Update on DQW crab cavity HOMs*, 140th HiLumi WP2 meeting, CERN, 29/01/2019.
140. V. Vlachodimitropoulos *et al.*, *Study of an Improved Beam Screen Design for the LHC Injection Kicker Magnet for HL-LHC*, in Proc. 8th Int. Particle Accelerator Conf. (IPAC'17),

Copenhagen, Denmark, May 2017, paper WEPVA094, pp. 3471–3474.

141. C. Bracco, *The new injection protection dump TDIS, Engineering Change Request*, LHC-TDIS-EC-0001, EDMS document 1936580, Jul. 2018. https://edms.cern.ch/document/1936580/.
142. E. Métral *et al.*, *Summary of the 2-day internal review of LHC performance limitations (linked to transverse collective effects) during run I (CERN, 25-26/09/2013)*. CERN-ACC-NOTE-2014-0006.
143. E. Métral *et al.*, *Summary of the half-day internal review of the LHC performance limitations (linked to transverse collective effects) during run II (CERN, 29/11/2016)*, CERN-ACC-NOTE-2017-0005.
144. X. Buffat *et al.*, *Transverse instabilities*, 9th Evian Workshop on LHC Beam Operation, Evian, France, 30 January – 1 February 2019.
145. E. Métral *et al.*, *Beam stability from impedance (including effect of coating) and overall summary for the nominal scenario including all effects*, 7th HL–LHC Collaboration meeting, Madrid, Spain, 13-16/11/2017.
146. G. Iadarola, *Digesting the LIU high brightness beam: is this an issue for HL–LHC?*, LHC Performance Workshop 2018, Chamonix, France, 29 January – 2 February 2018.
147. L.R. Carver *et al.*, *Transverse beam instabilities in the presence of linear coupling in the Large Hadron Collider*, Phys. Rev. Accel. Beams **21**, 044401 (2018).
148. X. Buffat, *Transverse beams stability studies at the Large Hadron Collider*, Ph.D. thesis, EPFL, Lausanne, Switzerland, 2015, doi:10.5075/epfl-thesis-6321.
149. E. Métral *et al.*, *Destabilising effect of the LHC transverse damper*, in Proc. 9th Int. Particle Accelerator Conf. (IPAC'18), Vancouver, BC, Canada, Apr.–May 2018, pp. 3076–3079. doi:10.18429/JACoW-IPAC2018-THPAF048.
150. K. Li *et al.*, *Electron cloud observations during LHC operation with 25 ns beams*, in Proc. 7th Int. Particle Accelerator Conf. (IPAC'16), Busan, South Korea, 8–13 May 2016, pp. 1458–1461. CERN-ACC-2016-255.
151. G. Rumolo *et al.*, *Electron cloud in the CERN accelerator complex*, in Proc. 57th ICFA Advanced Beam Dynamics Workshop on High-Intensity and High-Brightness Hadron Beams, Malmö, Sweden, 3–8 July 2016, Eds. D. Gous, M. Marx, R. Mueller (GSI, Germany), J. Olander, V.R.W. Schaa, G. Trahern, pp. 266–271. CERN-ACC-2016-0099.
152. K. Li *et al.*, *Update on Landau octupoles settings at injection*, 65th LHC Beam Operation Committee meeting, CERN, 23/08/2016.
153. A. Romano, *Electron cloud formation in CERN particle accelerators and its impact on the beam dynamics*, CERN-THESIS-2018-299.
154. A. Romano *et al.*, *Electron cloud buildup driving spontaneous vertical instabilities of stored beams in the Large Hadron Collider*, Phys. Rev. Accel. Beams **21** (2018) 061002.
155. N. Karastathis, *Dynamic Aperture at HL-LHC Injection*, presented at the 149th HiLumi WP2 Meeting, CERN, Geneva, Switzerland, May 2019, https://agenda.infn.it/event/823612.
156. G. Iadarola, *HPC for e-cloud computing*, 367th LHC Machine Committee, CERN, 07/11/2018.

157. S. Antipov *et al.*, *Impact of carbon coating on impedance and beam stability*, 124th HiLumi WP2 meeting, CERN, 03/07/2018.
158. W. Herr, *Features and implications of different LHC crossing schemes*, CERN, Geneva, Switzerland, LHC Project Report 628, 2003.
159. H. Grote, *Self-consistent orbits with beam-beam interactions in the LHC*, in Proc. EPAC 2000.
160. Train TWiki, https://twiki.cern.ch/twiki/bin/view/ABPComputing/TrainWikiPage.
161. A. Ribes Metidieri, *Studies of PACMAN effects in the HL–LHC*, 123th HiLumi WP2 meeting, CERN, 12/06/2018.
162. A. Ribes Metidieri and X. Buffat, *Studies of PACMAN effects in the HL–LHC*, in preparation.
163. S. White *et al.*, *Transverse mode coupling instability of colliding beams*, Phys. Rev. Accel. Beams **17**, 041002 (2014).
164. L. Barraud and X. Buffat, *Mode coupling instability of colliding beams in the HL–LHC*, in preparation.
165. L. Medina *et al.*, *Assessment of the performance of High Luminosity LHC operational scenarios: integrated luminosity and effective pile-up density*, Canadian Journal of Physics, https://doi.org/10.1139/cjp-2018-0291.
166. G. Iadarola, *HL–LHC filling schemes: possible optimization*, 140th HiLumi WP2 meeting, https://indico.cern.ch/event/788818/.
167. A. Valishev, S. Fartoukh and D. Shatilov, *BBLR compensation for HL–LHC*, 3rd Joint HiLumi LHC – 22nd LARP Collaboration Meeting, 7–8 May 2014, BNL, USA, https://indico.bnl.gov/event/730/contributions/17058/attachments/15282/18810/BBLR_Valishev-2014.05.08.pptx.
168. D. Banfi, J. Barranco, T. Pieloni, A. Valishev, *Update on crossing angle scaling with bunch intensity*, 20th HiLumi WP2 Task Leader Meeting, 25 October 2013, CERN.
169. D. Banfi, J. Barranco, T. Pieloni, A. Valishev, *Beam-beam effects for round and flat optics: DA simulations*, 4th Joint HiLumi LHC - LARP Annual Meeting, 17–21 November 2014, KEK, Japan, https://indico.cern.ch/event/326148/contributions/1711470/attachments/633056/871236/DaniloKEK.pptx.